Spring 5-2016

# Synthesis of Ferrocene-Oxadiazole Complexes and a Determination of Their LogD Values

Grace C. Gould
*University of Maine*

# SYNTHESIS OF FERROCENE-OXADIAZOLE COMPLEXES AND A DETERMINATION OF THEIR LogD VALUES

by

Grace C. Gould

A Thesis Submitted in Partial Fulfillment
of the Requirements for a Degree with Honors
(Chemistry)

The Honors College

University of Maine

May 2016

Advisory Committee:

Alice E. Bruce, Associate Professor of Chemistry, Advisor
Mitchell Bruce, Associate Professor of Chemistry
Raymond C. Fort, Jr., Professor of Chemistry
Carl P. Tripp, Professor of Chemistry and Director, Laboratory for Surface Science and Technology
Edith Elwood, Assistant Professor of Sociology, Honors College

## ABSTRACT

During the drug design process, there are many different approaches that researchers can take to improve the overall efficacy of a potential drug candidate. Aside from attempting to understand how different functional groups interact with target tissues, the physical properties of a particular molecule are also important determinants of overall effectiveness. If a molecule is too polar, it will display low permeability through the gastrointestinal tract, and will most likely be excreted through the body unchanged. Conversely, if a molecule is too nonpolar, it will be insoluble in blood and will display low distribution throughout tissues. This research describes attempts at the synthesis of multiple ferrocene-oxadiazole complexes, with an effort towards synthesizing compounds which display an aqueous solubility similar to candidates currently used in drug design. Oxadiazoles are a class of 5-membered, heterocyclic molecules which have attracted a tremendous amount of attention in recent years for their vast array of medicinal properties. Furthermore, the conjugation of ferrocene to bioactive molecules has demonstrated involvement with the suppression of cancer cells in mice. In this project, the aqueous solubility of one such ferrocene-oxadiazole complex was estimated using the LogD shake-flask assay, resulting in a value of 1.21. The results of an attempted synthesis of a more hydrophobic ferrocene-oxadiazole complex will be explained as well, along with a discussion of the challenges associated with different synthetic methods.

## TABLE OF CONTENTS

## LIST OF FIGURES

## LIST OF TABLES

## LIST OF SCHEMES

# 1. INTRODUCTION

This research is focused on attempts at synthesizing ferrocene molecules derivatized with an oxadiazole-containing sidechain. The method of preparation of the oxadiazole will be through a reaction of a ferrocene derivative with mercury (II) acetate, which has been shown to produce a ferrocene with a 1,3,4 oxadiazole-containing sidechain as the final product through a general mechanism similar to Scheme 1.[1]

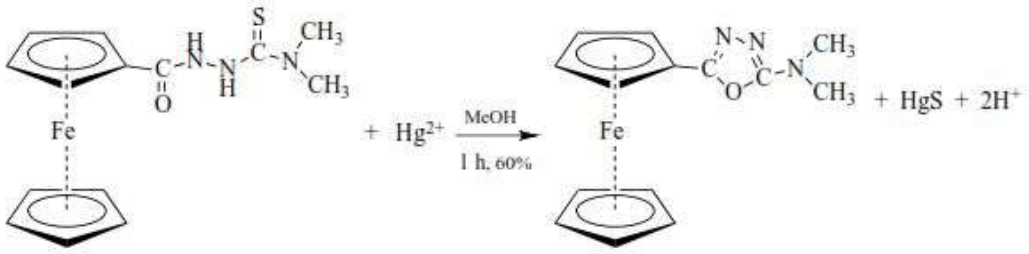


Scheme 1. Oxadiazole Synthesis[1]

When the same reaction with $Hg^{2+}$ occurs with different reactant structures, it is unknown whether or not cyclization of the final product will occur due to the selectivity of the reaction between the thiophilic mercury (II) ion and the thiosemicarbazide sidechain. Since there is a large amount of recent research discussing the potential medicinal applications of oxadiazole-containing drugs, including areas such as anticancer, anti-inflammatory, anti-microbial, and anti-viral medications, the goal of this research is to be able to synthesize a new compound which displays similar aqueous solubility and other physical properties to drug molecules currently used in a clinical setting.[2] A discussion of oxadiazoles, their properties and applications, as well as a basic overview of the principles which are involved in drug development will be given, as well as a brief experimental description.

## 1.1 Medicinal Properties of Oxadiazoles

Some of the most interesting compounds currently under investigation by medicinal chemists and pharmacologists are a group of heterocyclic molecules called oxadiazoles. Oxadiazoles consist of two carbon atoms, two nitrogen atoms, and an oxygen atom arranged in a five-membered ring, with double bonds connecting the carbon and nitrogen atoms. In their most stable form, oxadiazoles can exist as either the 1,2,4 (Figure 1) or the 1,3,4 (Figure 2) isomer. The isomers exhibit a significant variation in their physical and thermodynamic properties, both of which in turn affect their potential pharmaceutical uses[3].

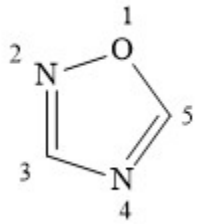


Figure 1. 1,2,4 oxadiazole

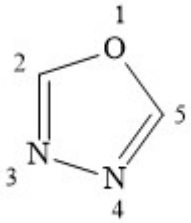


Figure 2. 1,3,4 oxadiazole

1,2,4 oxadiazoles are commonly synthesized from nitriles or a similar amidoxime derivative[4], while 1,3,4 oxadiazoles with various substitution patterns can be obtained from a reaction of acylhydrazides with acylating agents, or by dehydration of an acylsemicarbazide.[5]

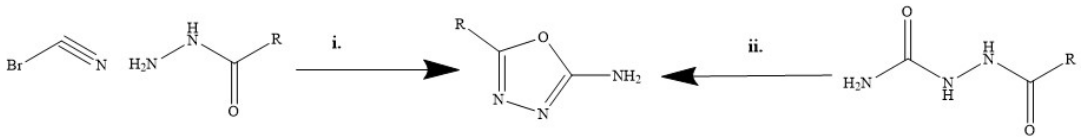


Scheme 2. 1,3,4 oxadiazole preparation via reaction of acylhydrazide with cyanogen bromide (i) and dehydration of acylsemicarbazide (ii).[5]

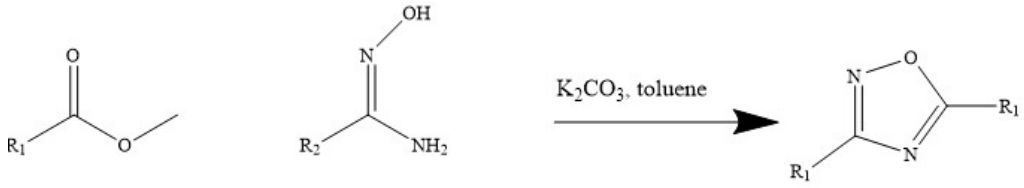


Scheme 3. 1,2,4 oxadiazole preparation from carboxylic esters and amidoximines.[4]

The differences in the structure of the 1,2,4- and the 1,3,4- isomers contribute heavily to a strong variation in physical properties. 1,3,4-oxadiazoles typically display much lower lipophilicity than the 1,2,4- isomers and a higher aqueous solubility, which can be attributed to the more pronounced dipole vector among the 1,3,4-oxadiazoles compared with the 1,2,4-oxadiazoles, as shown in Figure 3. Metabolic stability, which is a quantitative measure of the percentage of a compound degraded over time in the presence of a metabolically active system (such as the human body), was also shown to be greater in the 1,3,4- isomer verses the 1,2,4- isomer. Similar differences in activity are also demonstrated in the inhibition of cytochrome 450 enzymes, which are a class of enzymes involved in human liver microsome (HLM) metabolism. The 1,3,4- oxadiazoles display a much higher resiliency against HLM metabolism compared with that of the 1,2,4-oxadiazoles. In addition, the decreased inhibition of the hERG ion channel, which correlates to a decrease in lipophilicity, is also observed in the 1,3,4 oxadiazole compound. The differences in the physical properties of each isomer can be rationalized by the difference in charge distributions.[3]

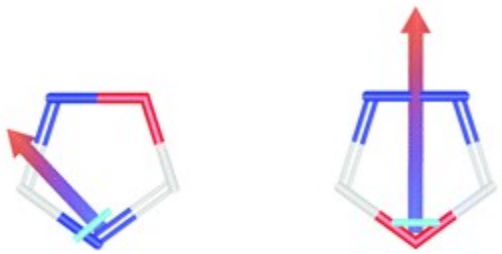

Figure 3. Charge distributions and dipole vectors of the 1,2,4- (left) and the 1,3,4-(right) oxadiazole isomers.[3]

Although there are several compounds containing oxadiazoles in late-stage clinical testing today, there exists one prominent oxadiazole-containing pharmaceutical currently being distributed. Raltegravir (Figure 4) is an integrase transfer inhibiting drug containing a 1,3,4-oxadiazole, approved by the FDA in 2011 for the treatment of

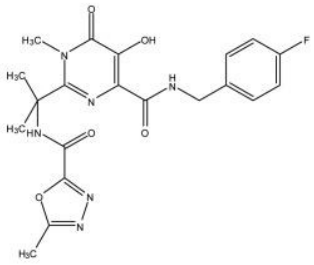

Figure 4. Raltegravir

human immunodeficiency virus (HIV) in both adults and children.[6] Raltegravir is both a potent and selective inhibitor of the strand transfer catalytic activity of one of the three enzymes involved in the replication of viral DNA. The outcome of treatment with Raltegravir is the prevention of viral DNA from integration into the human genome. In addition to the inhibition of HIV-1 replication, Raltegravir has also been shown to inhibit the infection of an additional twenty-three isolates of HIV-1, while maintaining selectivity in regards to the inhibition of human phosphoryl transferases, including DNA polymerases. The 1,3,4-oxadiazole, along with the fluorobenzene ring, assist in the

coordination of water molecules to HIV-1 integrase. Molecular thermodynamics studies have revealed that the two nitrogen atoms in the 1,3,4-oxadiazoles are favorable hydrogen bonding acceptors, even more than that of the oxygen atom in the ring, and as a result they are able to contribute favorably to the ligand interactions between the donor oxygen atom in water and the cationic portion of the enzyme. It is in this way that the water-mediated interaction with a positively-charged complex in HIV-1 integrase is believed to be an important factor in the inhibition of integrase activity and viral replication.[7]

In addition to its use as a hydrogen-bonding substituent in Raltegravir, 1,3,4-oxadiazoles are also being introduced into drug discovery programs for other purposes. Due to their ability to contribute favorably to ligand binding as discussed previously, 1,3,4-oxadiazoles are increasingly being incorporated into the pharmacophore (the components of a drug molecule which assist with coordination to the target site) due to their ability to mimic aromatic linkers and arrange substituents into a planar arrangement, as well as temperament of molecular properties through ligand-cation interactions. Due to their similar charge distributions, 1,3,4-oxadiazoles have been used as replacements for esters, amides, carbamates, and hydroxamide esters within various bioorganic structures.[3] Where smaller functional groups with similar charge distribution but lower metabolic stability have the potential to be metabolized rapidly by the enzymes in the human body, 1,3,4-oxadiazoles might be favored over those functional groups because of their more favorable metabolic stability.

## 1.2 Overview of Pharmacokinetic Parameters

In the process of determining a molecule's capacity for use as a drug, there are many factors to consider aside from metabolic stability, including bioavailability, the nature of the target site, toxicity and adverse side effects, potency, and pharmacokinetics.[8] Fundamentally, drug discovery programs seek to optimize the ADME (adsorption, distribution, metabolism, and excretion) properties of potential medicinal compounds, while simultaneously being able to balance potency of a drug with a reasonable dosing regimen. The pharmacokinetic profile of a drug describes how its effects within the body are compared with the amount of that drug remaining in circulation.[8] The four fundamental pharmacokinetic parameters necessary for characterizing a drug's passage through the body are clearance, volume of distribution, half-life, and bioavailability. The bioavailability of a drug is determined by the mode of administration, whether it be orally, intravenously, inspiratorily, etc.[9] It is defined as the fraction of an unchanged drug that is absorbed intact and reaches the site of action following administration[8]. The solubility of a compound has an effect on the preferred mode of administration, with an intermediate level of water solubility preferred for drugs which will be administered orally. Drugs which have lower water solubility/increased lipophilicity run the risk of decreased absorption following oral administration, and are extremely susceptible to rapid metabolism through hydrophobic absorptive surfaces of cell membranes. Conversely, drugs which are too soluble in water will have poor absorption across the gastrointestinal tract and will most likely pass through the body unchanged.[10] Drug solubility is determined by the thermodynamic relationships between the solute and the solvent, specifically, the energy required to overcome the strength of

intermolecular forces in the solute solid-state and the energy generated upon the interaction of solute and solvent. A polar molecule is able to dissolve in a polar solvent (i.e., water) because the strength of the interactions between the solute and solvent are much larger than the intramolecular interactions holding the solute and solvent molecules together. For nonpolar molecules trying to dissolve in a polar solvent, the strong covalent interactions holding the molecule together cannot be overcome by the interactions between solute and solvent, and so the solute remains as a precipitate in solution.[11]

There exist a number of strategies that chemists employ to improve the aqueous solubility of potential drug components. Suspension of the active ingredients in a drug within a medium of the optimal solubility properties, such as gel capsules, allows drug molecules which show poor water solubility to be dissolved in the capsule. When the capsule is ingested, it is metabolized by the body first, allowing the unchanged drug to be entered into circulation. Isolation of the salt forms of a drug, or its cocrystals, by modifying the suspension pH of a molecule enhances the solubility of a weakly acidic or basic drug in a polar solvent such as water.[12] In addition to these suspension techniques, modification of the drug structure itself with bioisosteres[13] (molecules with different physical properties which will produce the same biological outcomes) can also improve the solubility profile of a drug. In creation of the ferrocene/oxadiazole complex that this research aims to do, the structure of the starting thiosemicarbazide will be altered in order to change the aqueous solubility of the resulting molecule.

.

### 1.3 Properties and Applications of Ferrocene and its Derivatives

Ferrocene is an organometallic compound consisting of ferrous iron ($Fe^{2+}$) sandwiched between two flat, parallel cyclopentadienyl rings. It's "accidental" discovery in 1952 by researchers attempting to form a cyclopentadienyl radical through treatment with ferric chloride led to a renewed interest in organometallic chemistry and its subdisciplines, as well as the Nobel Prize in Chemistry for its discoverers. Today, its commercial availability and the ease with which the cyclopentadienyl rings can be functionalized has led ferrocene to be one of the most studied of the sandwich complexes.[14] As purchased, ferrocene is a yellowish-orange powder, which forms dark orange needle-like crystals upon sublimation. The compound itself can be easily modified through single electron oxidation reactions on the iron atom, electrophilic aromatic substitution on the cyclopentadienyl rings, or oxidized in the presence of acidic media to form stable, water-soluble ferrocenium salts. Owing to its favorable electrochemical properties, including high electron transfer rate, low redox potential, and stability of both ferrocene ($Fe^{2+}$) and ferrocenium ($Fe^{3+}$), ferrocene derivatives are frequently used as electrochemical sensors for DNA and proteins.[15] Furthermore, ferrocene is stable in a variety of biological media, yet lipophilic enough to penetrate cell membranes rapidly, it melts at 173 °C without prior decomposition, and it demonstrates a diversified mode of reaction with biological substrates.[16]

The bioactive properties of ferrocene derivatives and their potential medicinal applications are well-known. Ferrocene and its derivatives are shown to demonstrate antiproliferative, anticancer, and antimicrobial properties. Ferrocerone (shown in Figure

5**)** is an example of a ferrocene drug currently used in clinical practice which is used for the treatment of diseases linked to iron deficiency.[17]

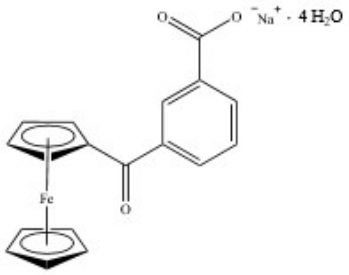


Figure 5. Ferrocerone[17]

Ferrocene-modified analogs of already prominent drugs including tamoxifen, which is used for the treatments of certain types of breast cancers, chloroquinone, which is used for the treatment of malaria, and other compounds which would otherwise have a high toxicity are currently undergoing clinical trials, with results demonstrating a similar if not improved potency over their commonly-used analogs.[18] The decreased toxicity and the decreased likelihood of adverse drug reactions with these ferrocene analogs compared with more-well known drugs is a major reason for their continued exploration. In general, acyl derivatives of ferrocene tend to be slightly more toxic than their alkyl counterparts.[19] Furthermore, the oxidized forms of ferrocene were shown to be more bioactive than the neutral ones, which may mean that the cytotoxic properties of these compounds depend on the ability of the derivatives to generate reactive oxygen species which can degrade the cellular components of the tumor or pathogen.[16]

### 1.4 Previous Work with Ferrocene-Oxadiazole Complexes

In previous work which explored the potential of using a ferrocene derivatized with a thiosemicarbazide for the detection of mercury (II) ion, the synthesis of a ferrocene/oxadiazole-containing compound was performed in two major steps: the reaction of ferrocene monocarboxylic acid with a thiosemicarbazide and the subsequent reaction of that structure with mercury (II) acetate.[1] The reaction scheme of the ferrocene with the thiosemicarbazide and the subsequent attack of the sulfur with the mercury (II) ion are shown in pathways **(i)** and **(vi)** of Scheme 4 on page 12. The carboxylic acid of the ferrocene and the amide of the thiosemicarbazide are joined via amide coupling with HBTU, resulting in the formation of peptide bond and the expulsion of water from the compound. The second step shows the attack of the mercury on the sulfur, the precipitation from solution of HgS, and the subsequent cyclization of the sidechain to form the molecule of interest: a 1,3,4 oxadiazole.

This research aims to build upon previous work by reacting the same starting material, ferrocene monocarboxylic acid with a series of different thiosemicarbazides. The goal of this research is to determine whether the reactions between the sulfur and the mercury can still occur and afford a cyclized oxadiazole product under the same conditions as the aforementioned schemes. The thiosemicarbazides will be selected on the basis of containing groups that enhances the medicinal properties of the entire molecule, including improvement of the molecule's pharmacokinetic profile[8], aqueous solubility[12], or metabolic stability.[20]

A careful investigation and selection of the thiosemicarbazides is of the utmost importance in order to carry out the derivatization of the ferrocene and the formation of a

novel ferrocene-oxadiazole compound. A general procedure would involve the systematic selection and testing of a variety of thiosemicarbazides to see, first and foremost, whether or not functionalization of the ferrocene can occur and whether or not the resulting structure can be worked up to produce an oxadiazole. The influence of a sulfur and peptide structure which reacts with the ferrocene has been shown to have little effect on the rate at which HgS precipitates out of solution, a phenomenon which has not been observed with other metal cations.[21] Additionally, the cyclization of acylthiosemicarbazides to oxadiazoles stemming from a reaction with mercury (II) has been shown to occur under mild reaction conditions, with the achievement of high yields of oxadiazoles.[22] The precipitation of HgS out of the reactant and the subsequent oxadiazole formation is a thermodynamically favorable process, and therefore should occur under a variety of reaction conditions. Therefore, the biggest challenge facing this research is most likely to arise during the amide coupling portion of the synthesis.

Ultimately, the employment of spectroscopic techniques will be used to determine the nature of the final product. Proton nuclear magnetic resonance spectroscopy will be used to elucidate the structure and chemical environment of certain molecules by measuring the response of a nucleus to a change in an external magnetic field, quantized through a value known as chemical shift. Chemical shifts are a characteristic of certain functional groups, and the peak splitting patterns of those shifts and integral values can be used to elucidate the structure of the product being analyzed.

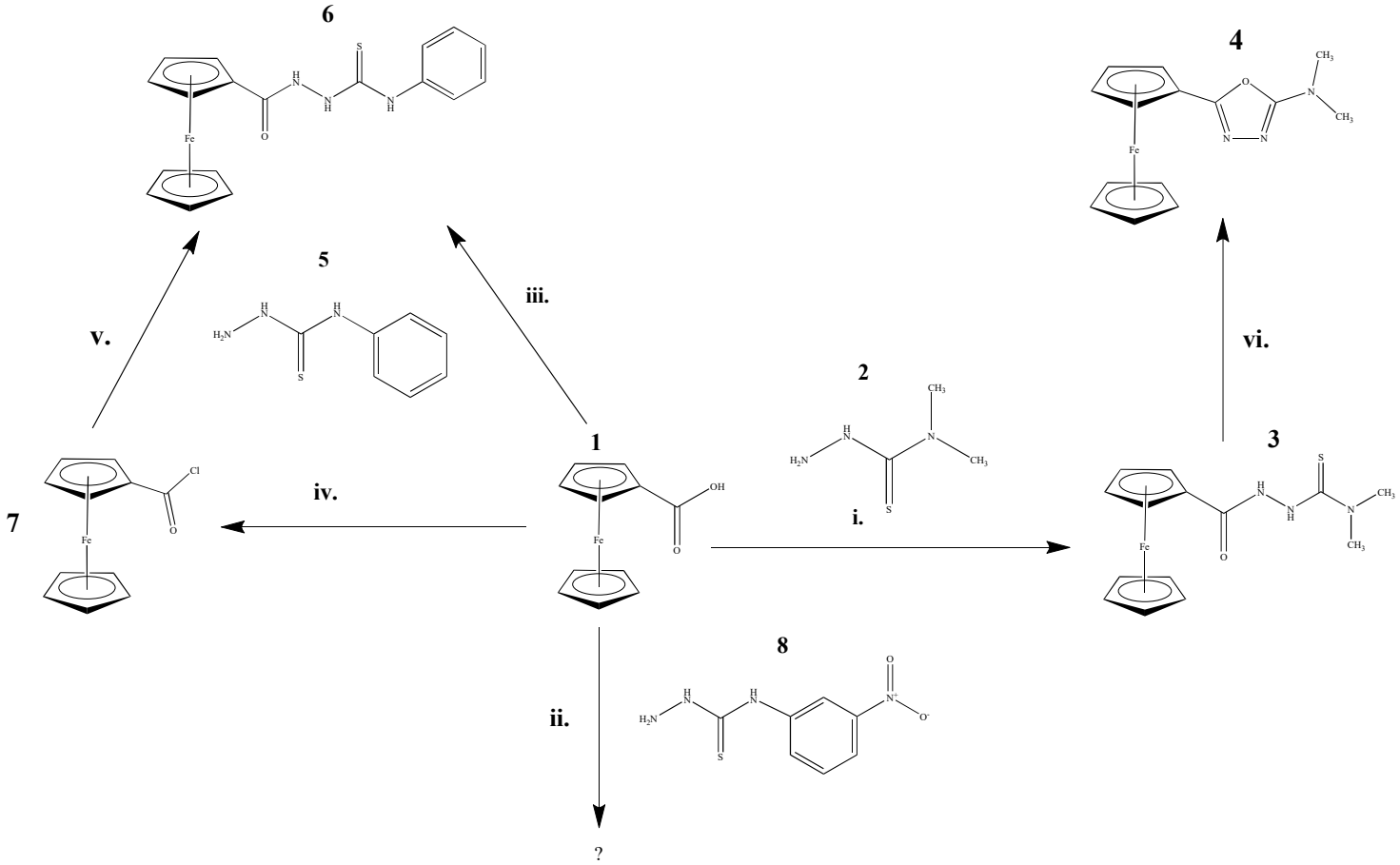


Scheme 4. Structures of starting materials and products used for synthesis. **(i), (ii), (iii):** HBTU/triethylamine, 24 hrs. in acetonitrile. **(iv):**oxalyl chloride/pyridine cat., 2 hrs. in methlylene chlroride. **(v)**:triethylamine, 16 hrs. in acetonitrile **(vi):** mercury acetate, 1 hr. in methanol.

### 1.5 Partition Coefficients and Lipophilicity

In addition to attempting to synthesize a novel oxadiazole-containing compound, the lipophilicity of each compound will also be determined. Lipophilicity is one of the key determinants of the pharmacokinetic behaviors of a drug, affecting the absorption of the drug into cells and tissues, the binding characteristics of the drug, and the solubility of the drug in blood, cerebrospinal fluid, and other media which are common medicinal targets. Therefore, an accurate determination of the lipophilicity of potential drug candidates is a high priority for medicinal chemists undertaking a drug design process. One of the oldest but most commonly used *in vitro* methods for determining the lipophilicity of any compound is by measuring an organic-aqueous partition coefficient of the compound.[23] These values are typically reported as a numerical LogD, which is calculated according to the formula:

$$LogD = log\left(\frac{C_{organic}}{C_{aqueous}}\right)$$

1-octanol and water are generally accepted as the most accurate two-phase system for modeling the partition coefficient between tissues and blood. The aqueous solution usually consists of a phosphate buffer prepared to pH 7.4 (the physiological pH of blood), and 1-octanol is the solvent that most closely mimics the chemistry of the phospholipid bilayer of cell membranes.[24] The distribution of the compound in each phase can be determined using a variety of methods, but most commonly, the shake-flask or stir-flask assay. In these methods, a small amount of the compound of interest is dissolved in a polar aprotic solvent (usually dimethyl sulfoxide), and then mixed in a test tube or vial containing equal portions of 1-octanol and aqueous buffer. The tube is then shaken for a period ranging from 2-24 hours, allowing the compound to equilibrate between the two

phases. After the shaking is complete, the phases are separated from each other and the concentration of the compound is analyzed using UV-Visible spectroscopy, HPLC, UPLC, or other analytical means.[23]

The optimal LogD value for a particular drug varies on the region of the body that drug is targeting, as shown in Table 1 below.

Table 1. LogD values and their associated outcomes *in vivo*.[25]

| LogD Value | Solubility in Blood | GI Absorptivity |
|---|---|---|
| <0 | High | Low |
| 0-1 | High | High |
| 2 | Average | Average |
| >5 | Low | High |

Generally speaking, a compound will have a good balance between solubility in fluids and permeability through cell membranes if the LogD value is in the range from 0-3. For drugs which need to cross the blood-brain barrier, the LogD value should be somewhere around 2. Hydrophilic compounds have a LogD close to 0 will be readily soluble in blood but exhibit low permeability across the gastrointestinal tract or blood-brain barrier. Highly lipophilic compounds are those which have a LogD greater than 5, and are poorly soluble in blood, resulting in a high degree of plasma protein binding, resulting and extremely low oral bioavailability.[25]

## 2. MATERIALS AND METHODS

**Reagents.** Ferrocene monocarboxylic acid (97%) was purchased from Strem Chemicals, Inc.. Acetonitrile, ethyl acetate, methanol, ethyl ether anhydrous, methylene chloride, and monobasic potassium phosphate (USP Grade) were all purchased from Fisher Scientific. Triethylamine (99.5%), N,N,N′,N′-Tetramethyl-O-(1H-benzotriazol-1-yl)uronium hexafluorophosphate (HBTU, <98%), 4,4-dimethyl-3-thiosemicarbazide (98%), mercury (II) acetate (>98%), 1-octanol, oxalyl chloride ( ≥99%), 4-phenylthiosemicarbazide (99%), 4-(3-nitrophenyl)-3-thiosemicarbazide, pentane, pyridine, dimethyl sulfoxide, and dibasic potassium phosphate (USP Grade) were all purchased from Sigma-Aldrich. Deuterated dimethyl sulfoxide, d-acetonitrile, and d-chloroform (99%) were purchased from Cambridge Isotope Laboratories, Inc. for use in proton NMR. Air-sensitive experiments were conducted under an atmosphere of pre-purified nitrogen gas. All reagents used met or exceeded ACS Grade purity, and required no additional purification steps prior to use.

**Instrumentation.** A Varian Unity Plus Oxford 400 MHz NMR was used for all $^{1}H$ NMR experiments. UV-Vis experiments were performed on a Perkin Elmer Lambda25 Spectrophotometer. All compounds were weighed using a Mettler AE50 analytical balance.

### 2.1 Synthesis of 1-ferrocenoyl-4,4-dimethyl-3-thiosemicarbazide (Compound 3).

Ferrocene monocarboxylic acid, **1**, **(**0.5718 g, 2.5 mmol) was dissolved in 25 mL of acetonitrile in a 150-mL Erlenmeyer flask. The flask was equipped with a magnetic stir bar and stirred for 1 minute to promote dissolving of the solute. Triethylamine (180

μL, 2.5 mmol) was added to this solution, causing a color change from a pale orange to deep red. HBTU (0.9526 g, 2.5 mmol) was added directly to the flask and allowed to stir for 15 minutes. 4,4-dimethyl-3-thiosemicarbazide, **2**, (0.2998 g, 2.5 mmol) was then added to the flask, along with an additional 180 μL of triethylamine, before the flask was capped and allowed to stir for an additional 24 hours. During that time, the color of the solution changed from a very deep red to a dark brown.

Following the 24-hour stir period, the flask was removed from the stir plate. The solution in the flask was a deep brown color, with visible light brown precipitate settled on the bottom of the flask. The acetonitrile was decanted from the flask, and the remaining precipitate was washed twice with 30 mL of ethyl acetate. The ethyl acetate was added to the flask, swirled gently for 30 seconds, and then the resulting brown liquid drawn out of the flask with a Pasteur pipette, leaving behind a light brown powder. After the second wash, the powder was dissolved in 10 mL of dimethyl sulfoxide, and re-precipitated using 5 mL of distilled water. The addition of the water to the organic solution caused bright-orange solids to aggregate in the bottom of the flask. The solution was filtered with a long-stem funnel and the precipitate was left to dry on the filter paper.

After 48 hours of drying, the crude product, **3**, (0.54 grams, 60%) was recrystallized in methanol. The tan precipitate was transferred from the filter paper to a 150-mL Erlenmeyer flask containing 80 mL of methanol. The flask was then submerged into a beaker on a hot plate containing distilled water, and the methanol was heated to boil for approximately 15 minutes, with the flask being occasionally removed from the beaker and swirled to prevent buildup of precipitate on the walls of the flask. After all of the product had dissolved in the methanol, the solution was filtered hot through a long

stem funnel. The resulting orange filtrate was collected in a 100 mL Erlenmeyer flask and returned to the hot water bath, where the methanol was allowed to boil off of the solution. After 20 minutes, the solution had condensed enough where some small reddish-orange crystals were visible in the flask. The solution was removed from the hot water bath and allowed to cool to room temperature before being submerged in a beaker of crushed ice in the freezer. Following crystal formation after approximately 30 minutes in the ice bath, the liquid was decanted from the flask and the remaining reddish-orange crystals were washed with 5 mL of cold methanol five times. After the fifth wash, the methanol remained almost clear after swirling the crystals. The crystals in the flask were dried by lightly blowing nitrogen gas on the surface of the crystals from a needle. The crystals were then allowed to dry in a desiccator for 48 hours before weighing (0.055 g, 6%) and spectroscopic analysis using $^{1}$H NMR.

**2.2 Synthesis of N,N-dimethyl(5-ferrocenoyl-1,3,4,-oxadiazol-2-yl)amine (Compound 4).**

Recrystallized Compound **3** (0.05 grams, 1.5 mmol) was placed into a 150-mL Erlenmeyer flask and set to stir on a magnetic stir plate with 90 mL of methanol. Once the ferrocene had dissolved, mercury (II) acetate (0.479 grams, 1.5 mmol) was added to the flask, and the solution was allowed to stir for 1 hour. Following the stir period, the solution was transferred to a 100 mL Schlenk flask, and the methanol was evaporated using a vacuum pump. Once all of the solvent had been evaporated, the remaining yellowish-brown residue on the walls of the flask was suspended in 10 mL of anhydrous ethyl ether, and then filtered using gravity filtration in a long-stem funnel. The orange filtrate was collected in a Schlenk flask and dried again using the vacuum pump.

To purify the final product and to remove any unreacted starting material, the dried product was extracted twice with distilled water. Ethyl acetate (50 mL) was added to the Schlenk flask to dissolve the product, and the resulting yellow solution poured into a 125 mL separatory funnel. Distilled water extractions of 50 mL were performed twice, and the aqueous layer was discarded. The organic layer, which was a bright yellow color, was poured into a beaker and left to dry for 24 hours. Returning to the beaker the next day, all of the ethyl acetate had evaporated off, leaving behind a series of small, red spindle-shaped crystals. The crystals, **4**, (0.0035 grams, 7%) were easily scraped from the bottom of the flask, and analyzed using $^{1}$H NMR.

### 2.3 LogD Determination of Oxadiazole

Recrystallized Compound **4** (0.0035 grams) was dissolved in 50 µL of dimethyl sulfoxide, and pipetted into a vial containing 1000 µL of 1-octanol and 1000 µL of 10 mM aqueous phosphate buffer adjusted to pH 7.4. The buffer was prepared by combining potassium phosphate monobasic (0.0152 grams, 0.11 mmol) and potassium phosphate dibasic (0.0680 grams, 0.39 mmol) in a 100 mL volumetric flask and diluting to the mark with distilled water. To compensate for the absence of a mechanical shaker, the vial containing the compound and both phases was capped and shaken manually for one hour before being placed in the centrifuge for five and a half hours. The tube was removed from the centrifuge and the aqueous (bottom) and organic (top) layers were separated from each other using a separatory funnel. The two solutions were then transferred separately to a 1 mL cuvette and analyzed using UV-Visible spectroscopy. Prior to obtaining the scans of the phases, the machine was blanked using a cuvette containing 1

mL of 1-octanol and another containing 1 mL of the phosphate buffer. The scans for **4** in each of the two phases were superimposed and are shown in Figure 25 of the Results section.

In order to determine the concentrations in each of the phases, calibration curves of **4** in both 1-octanol and phosphate buffer were constructed in order to calculate the extinction coefficient in each solution. The procedures for making each calibration curve was identical. Compound **4** (2 mmol) was dissolved in 50 μL of dimethyl sulfoxide, and then suspended in 3.5 mL of the solution being analyzed. This initial concentration of 2 mM was analyzed using UV-Vis spectroscopy. The subsequent four dilutions were made through serial dilutions. In order to gauge the responsiveness of absorbance to changes in concentration, the second dilution was prepared by drawing 3 mL of the stock solution into a 5-mL syringe and diluting that solution to a new concentration of 1.7 mM by adding 0.5 mL of 1-octanol or buffer. After this second scan, the subsequent three dilutions were made through a twofold dilution procedure. The more concentrated solution was combined with buffer/octanol in a 1.75 mL to 1.75 mL ratio, until five total dilutions for each phase were scanned. The results for each phase were completed in triplicate, using the same quantity of starting material. The three scan results for each phase are shown in Figures 17-22. The calibration curves for each phase were made by plotting the absorbance at the maximum wavelength (444 nm) as a function of the average concentration between the three trials, and are shown in Figures 23 and 24.

### 2.4 Attempted Synthesis of 1-ferrocenoyl-4-phenylthiosemicarbazide (Compound 6) via HBTU Coupling

Compound **1** (0.19 grams, 1.7 mmol) was dissolved in 10 mL of acetonitrile and placed in a 100-mL Erlenmeyer flask equipped with a stir bar. As the solution was being stirred, triethylamine (60 µL, 1.7 mmol) was added to the solution, changing the color from a bright orange to a red. To this stirring solution, HBTU (0.316 grams) was added, and the solution continued to stir at room temperature for 20 minutes. Following the stir period, 4-phenylthiosemicarbazide, **5**, (0.14 grams, 1.7 mmol) was added, along with another 60 µL aliquot of triethylamine. The flask was capped and allowed to stir at room temperature for 24 hours.

After the overnight stir period, the flask was examined for precipitate buildup. Over the course of the stir period, a dark brown precipitate had built up along the walls of the flask, and the liquid portion had turned a dark brownish-green color. The contents of the flask were washed with ethyl acetate (30 mL x 3), and the remaining liquid drawn off and put into another beaker. The residual brown precipitate was then diluted with approximately 15 mL of DMSO and 10 mL of water. Unlike previous synthesis attempts, the addition of water did not cause the precipitation of solid out of the DMSO. A solvent extraction of diethyl ether (25 mL x 2) was attempted on the DMSO solution, but the product remained dissolved. Additionally, another 25 mL of water was added to the DMSO solution to try and drive out the precipitate, but no solids had formed after an hour in the ice bath. After a failed attempt to remove the liquid using a vacuum pump, the solution was discarded.

Recovery of the product from the acetonitrile/ethyl acetate extracts from the initial reaction solvent was accomplished by pouring the solution into a flask, submerging the flask in a beaker of cold water, and cooled in the refrigerator overnight. In the morning, some brown precipitate identical to the precipitate in the flask was observed following the 24-hour stir period. The liquid was drawn out of the flask, and the solid product was washed with hexanes (10 mL) and diethyl ether (10 mL x 2). The solid was dried using a needle blowing nitrogen gas, and the crude product (0.05 grams) was analyzed using $^{1}$H NMR. The remaining product was recrystallized in hot methanol, leaving behind a very small amount (< 0.003 grams) of fine, orange needles, **6**, that were analyzed using $^{1}$H NMR.

A second procedure with double the quantities of starting materials was attempted as well with a modified workup procedure. The ethyl acetate/acetonitrile washes obtained following the stir period were dried *in vacuo*, leaving behind a thick, gooey residue on the interior of the Schlenk flask. The residue was washed with diethyl ether (25 mL x 3), and the bright orange ether fractions were pooled in a beaker and set aside to dry. The remaining residue in the flask was dissolved in methanol, and a recrystallization was attempted. During the heating process, the methanol solution turned a clear deep red, and during filtering, a large quantity of black/brown precipitate was retained on the filter paper. Following filtration, the filtrate was once again heated to evaporate some of the methanol. Once the volume had been reduced to approximately 5 mL, and no condensation of the product has occurred in the solution, 5 drops of distilled water were added to the flask and reheated. The addition of water yielded a black/brown precipitate, which was isolated from the liquid using a Büchner funnel and analyzed using $^{1}$H NMR.

The ether extracts, after drying in a vacuum, yielded an orange oil on the walls of the flask. The oil was analyzed using $^{1}$H NMR, and an attempted recrystallization of the residue in methanol yielded the same blackish/brown powder identical to the other extracts.

### 2.5 Attempted Synthesis of Compound 6 Using a Carbonyl Chloride Intermediate

The preparation of ferrocene carbonyl chloride was adapted from a similar procedure by Lapic et. al.[26] The synthesis was conducted under a nitrogen atmosphere. Compound **1** (600 mg, 2.6 mmol) was dispensed into a Schlenk flask equipped with a stir bar and an exit needle. The exit needle was connected to a solvent trap, and, with a second needle, nitrogen gas was blown into the flask for 5 minutes to remove excess air and moisture. Simultaneously, 30 mL of methylene chloride were dispensed into a round-bottom flask, and nitrogen gas was bubbled through the liquid for 15 minutes. Using a cannula, approximately 15 mL of the degassed (oxygen and water-free) methylene chloride was transferred to the Schlenk flask. Using a plastic syringe, 0.54 mL of oxalyl chloride were dispensed through the septa into the flask, along with 2 drops of pyridine, causing the solution to turn from a pale yellow to a dark red and bubble vigorously. The flask was then connected to a condenser, and allowed to gently reflux for two hours on a heating mantle. Following the reflux period, the contents of the flask were dried *in vacuo* to yield a dark red oil. The oil was gently heated on the mantle and washed with petroleum ether (15 mL x 3) and pentane (10 mL x 2). The resulting blackish-brown residue was discarded, and the dark red extracts were pooled and dried again *in vacuo* to yield another red oil. In order to estimate a mass of the oil for further synthetic steps, the

oil was re-dissolved in methylene chloride, poured into a flask of known weight, and evaporated. A small portion of this re-evaporated compound, was used for $^{1}$H NMR.

The product, ferrocene carbonyl chloride, **7**, (0.553 grams, 2.22 mmol) was redissolved in 15 mL of methylene chloride and set to stir on a magnetic plate. A solution of Compound **5** (0.37 grams, 2.22 mmol) dissolved in 10 mL was poured into the carbonyl chloride along with triethylamine (0.69 mL, 5 mmol). The solution was covered with a septum and allowed to stir for 24 hours. The resulting dark brown-reddish liquid in the flask was transferred to a separatory funnel and extracted with a saturated sodium bicarbonate solution (20 mL x 3), followed by a wash with distilled water (20 mL x 2). The yellow extracts of the aqueous layer were pooled and left to dry. The brown organic layer was dried *in vacuo*, suspended in methanol, and recrystallization was attempted. Although some of the residual powder immediately dissolved in the methanol upon heating, the methanol solution still appeared slightly cloudy even after the methanol had been heated to its boiling point. The first filtering of the solution yielded a yellow filtrate, with a large amount of black powder retained on the paper. The black powder was reserved for $^{1}$H NMR. The yellow filtrate was heated slowly to boiling, filtered again, and then both solutions were dried *in vacuo* and analyzed using $^{1}$H NMR.

### 2.6 Attempted Synthesis of 1-ferrocenoyl-4-(3-nitrophenyl)-3-thiosemicarbazide

Compound **1** (0.023 grams, 0.43 mmol) was dissolved in 10 mL of acetonitrile and 15 μL of triethylamine (0.43 mmol) and stirred on a magnetic plate. HBTU (0.43 grams, 0.43 mmol) was added to this mixture and allowed to stir for 15 minutes. After stirring, 4-(3-nitrophenyl)-3-thiosemicarbazide, **8**, (0.092, 1.75 mmol) were added to this solution along with another 15 μL aliquot of triethylamine, and the solution continued to stir covered for 36 hours. After the stirring period, the dark brown liquid contents of the flask were removed with a Pasteur pipette, and the residual beige solid was diluted with 10 mL of ethyl acetate and withdrawn. The ethyl acetate wash was repeated two more times, during which the wash color changed from dark brown, to yellow, to almost colorless by the third wash. The pale orange precipitate was dried using nitrogen dispensed from a needle, and analyzed using $^{1}$H NMR. The precipitate was then recrystallized using methanol, yielding bright orange crystals which were analyzed using proton NMR.

# 3. RESULTS AND DISCUSSION

## 3.1 Synthesis of Oxadiazole

Figures 6-11 show the structures and NMRs of the starting materials used in the synthesis of the compounds shown in Scheme 4. Since the $^{1}H$ NMR of each compound in this synthesis was taken in DMSO-d6, all of the spectra contain a solvent peak at 2.5 ppm, with a water peak appearing in the spectra at 3.3 ppm. Ferrocene monocarboxylic was the only starting material stored at room temperatures. HBTU and 4,4-dimethyl-3-thiosemicarbazide were stored in plastic bags in the refrigerator due to air-sensitivity. The peak assignments and integrations for all three starting materials are shown in Table 2.

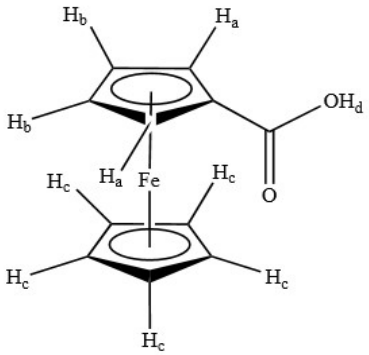


Figure 6. Structure of Compound **1**.

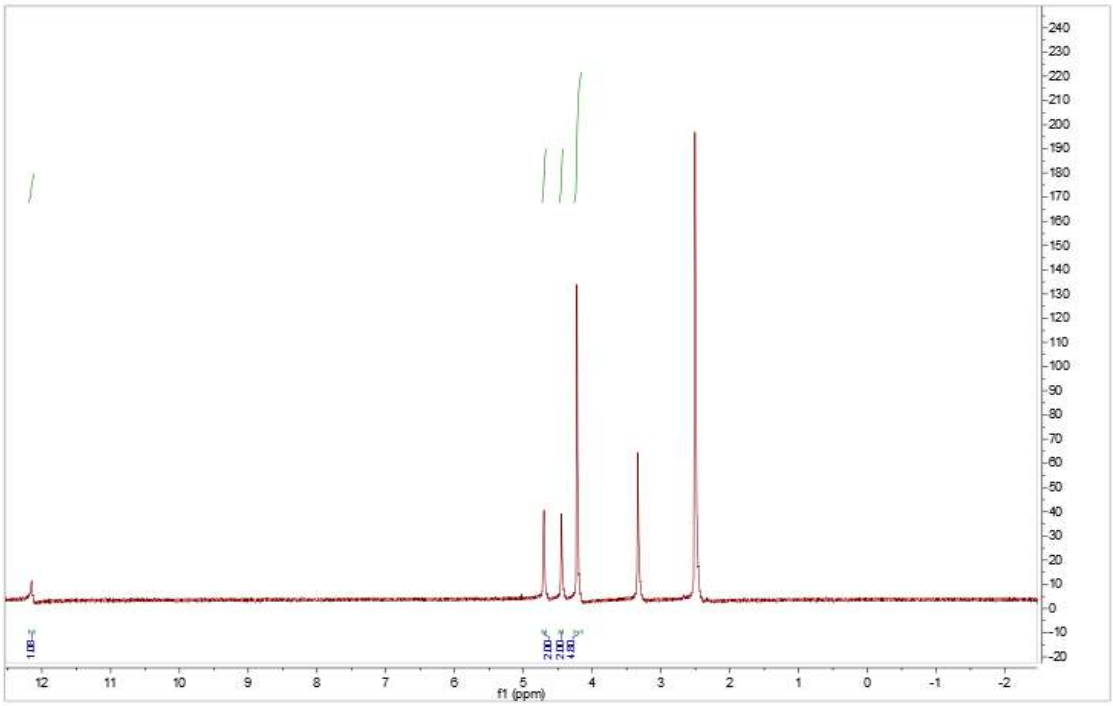


Figure 7. $^{1}$H NMR of Compound **1** in DMSO-d6

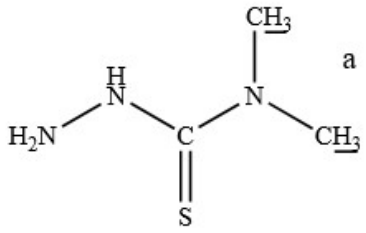


.

Figure 8. Structure of Compound **2**.

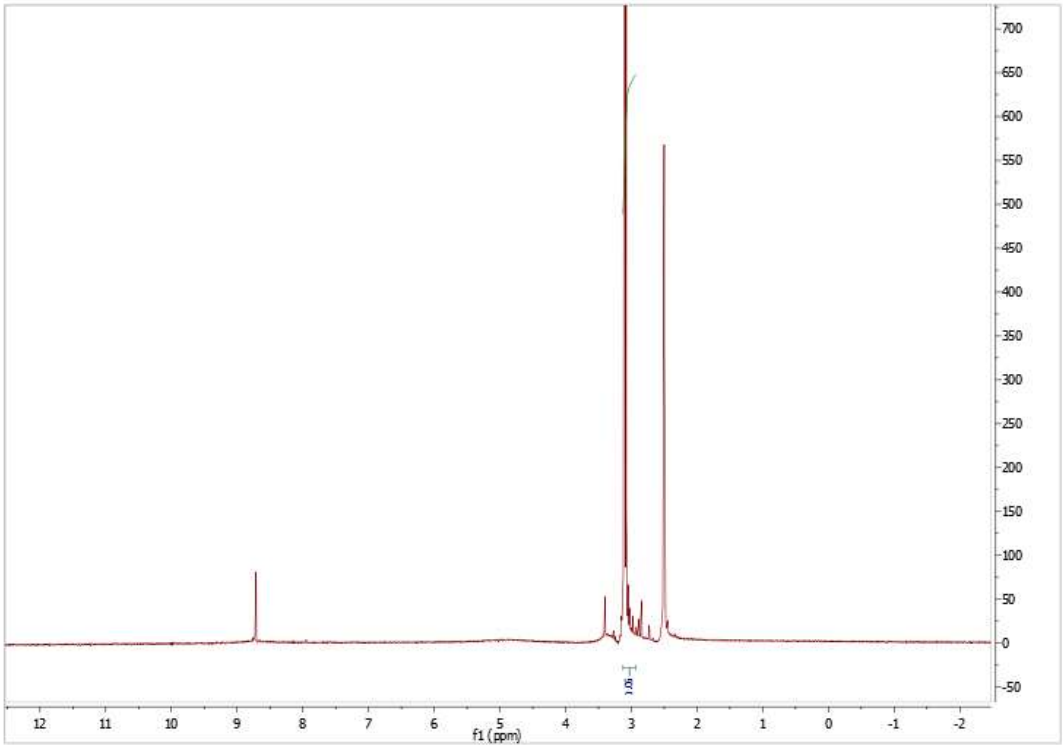


Figure 9. $^{1}$H NMR of Compound **2** in DMSO-d6.

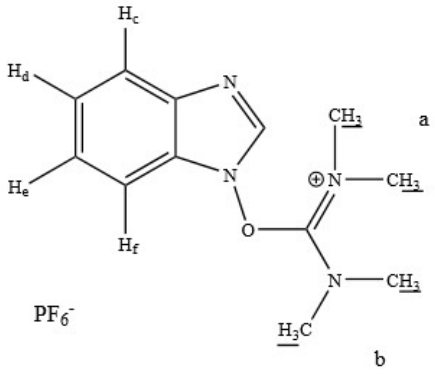


Figure 10. Structure of HBTU

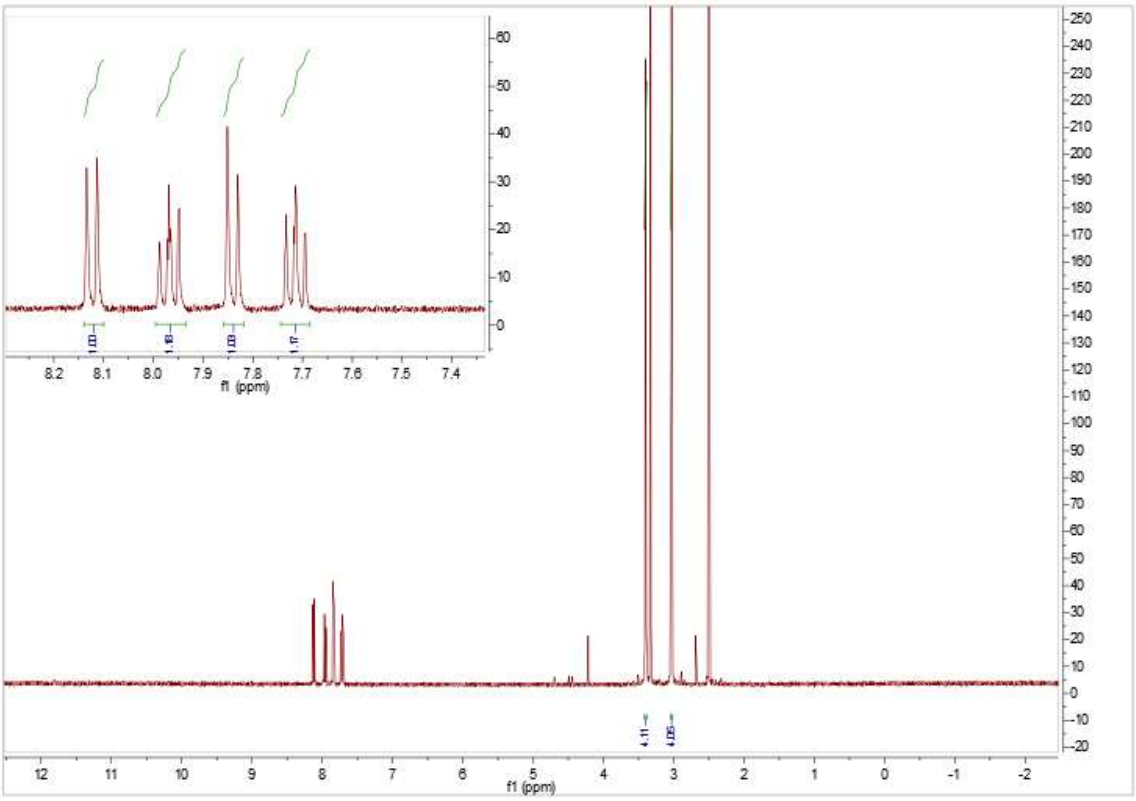


Figure 11. $^1$H NMR of HBTU in DMSO-d6.

As evidenced by the three small peaks in the 4-5 ppm range which are characteristic of a monosubstituted ferrocene, there was a small amount of contamination in this particular bottle of HBTU from the ferrocene monocarboxylic acid. This impurity persisted in the NMR even though multiple scans of different HBTU samples were taken,

meaning that the impurity was likely present in the entire bottle of HBTU. The trace amounts of Compound **1** in the HBTU, however, did not have any noticeably adverse effects on the synthesis.

Table 2. Chemical shifts of starting materials used in preparation

| | **Assignment** | **Chemical Shift (ppm)** | **Integration** | **Theoretical Integration** |
|---|---|---|---|---|
| **Compound 1** (Figure 7) | $H_a$ | 4.22 (s) | 4.80 | 5 |
| | $H_b$ | 4.44 (t) | 2.00 | 2 |
| | $H_c$ | 4.71 (t) | 2.00 | 2 |
| | $H_d$ | 12.15 (bs) | 1.00 | 1 |
| **Compound 2** (Figure 9) | $H_a$ | 3.10 (s) | 6.00 | 6 |
| **HBTU** (Figure 11) | $H_a$ | 3.40 (s) | 4.11 | 3 |
| | $H_b$ | 3.03 (s) | 4.05 | 3 |
| | $H_c$ | 8.12 (dt) | 1.00 | 1 |
| | $H_d$ | 7.71 (m) | 1.17 | 1 |
| | $H_e$ | 7.85(dt) | 1.03 | 1 |
| | $H_f$ | 7.97 (m) | 1.18 | 1 |

Since none of the starting materials underwent any type of purification process, the integration values did not exactly match the theoretical values expected based on assignment of nonequivalent protons. These discrepancies with the integration did not change the overall outcomes of the synthesis as it proceeded.

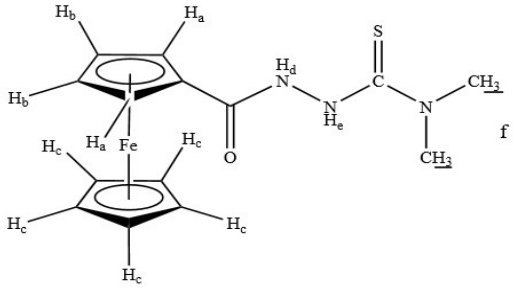


Figure 12. Structure of Compound **3**.

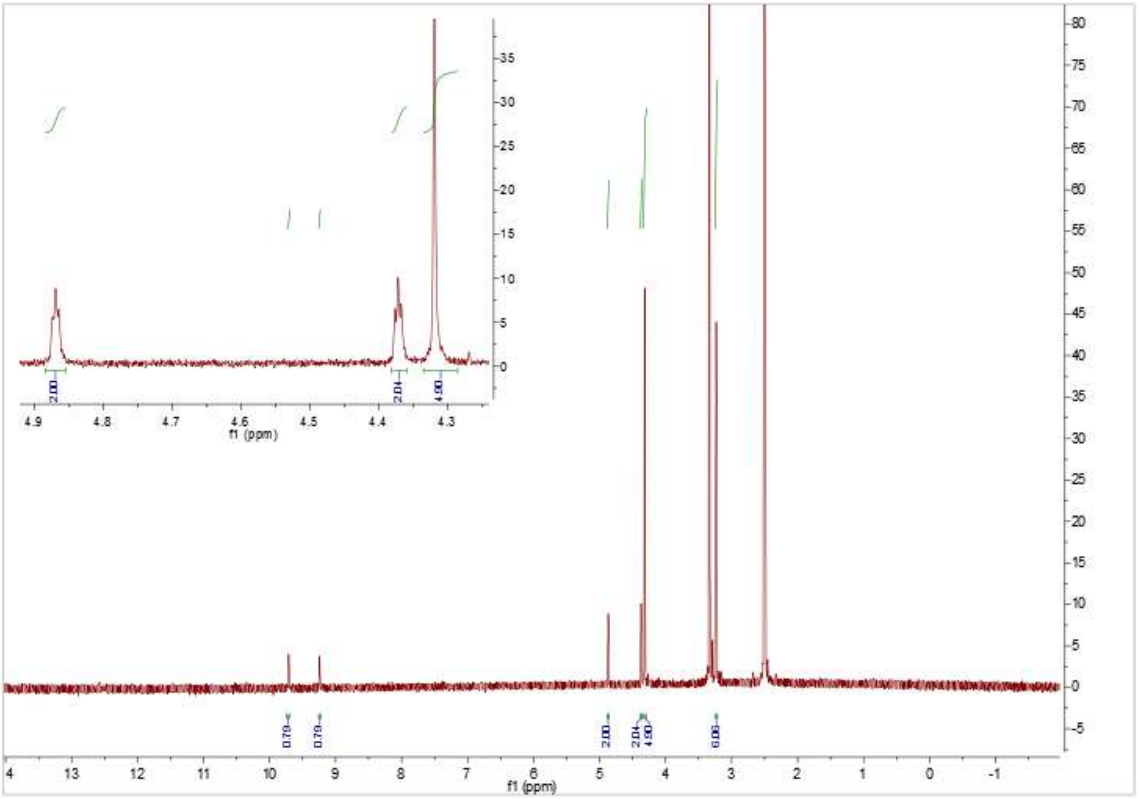


Figure 13. $^{1}$H NMR of crude Compound **3** in DMSO-d6.

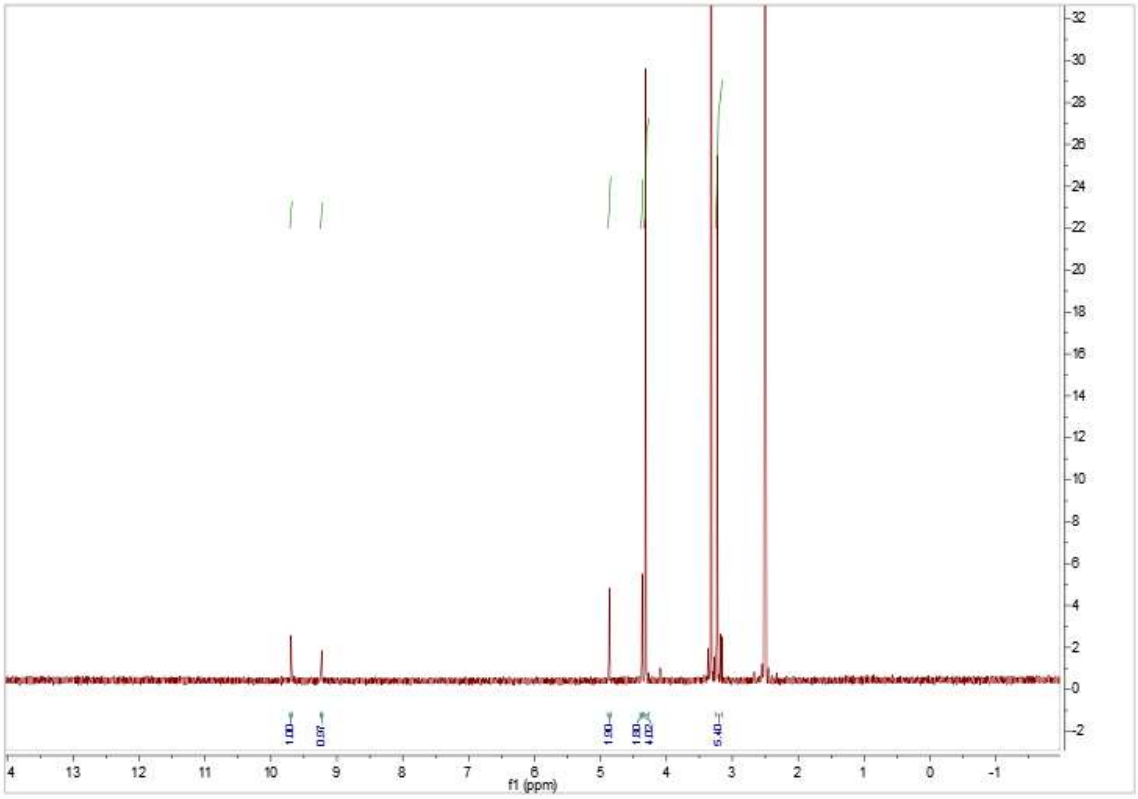


Figure 14. $^{1}$H NMR of Compound **3** (recrystallized in methanol) in DMSO-d6

Based upon what is known about the reaction mechanism between the ferrocene reactant and the thiosemicarbazide, the only peak that ought to have disappeared between the structures of the starting materials and the reactants is the OH proton, which appeared at 12.15 ppm in the NMR shown in Figure 7. As shown in Figures 13 and 14, that peak did disappear, meaning that the dehydration reaction did occur and a new amide bond was formed. The NMRs of the products also displayed two new singlets between 9 and 10 ppm. These singlets represent the two nonequivalent -NH groups formed during the dehydration reaction. The most downfield singlet signifies the -NH proton closest to the carbonyl carbon, positioned so due to greater deshielding  by the more electronegative oxygen compared with the sulfur. The spacing between the peaks of the monosubstituted ferrocene also decreased, in particular, the peaks showing the five unsubstituted

cyclopentadienyl ring protons and the two equivalent protons furthest away from the carbonyl group. This difference in spacing occurs due to the increased shielding of the protons on the unsubstituted Cp ring due to a less polar side chain on the ferrocene. Since the bulky thiosemicarbazide now attached to the ferrocene has some electron-donating properties, the $H_b$ protons appear more upfield than they did in the starting material.

The differences between the crude product and the recrystallized product are minimal. The only observable difference between these two spectra is the emergence of a small singlet around 3.1 ppm in Figure 14, just upfield from the water peak. This trace impurity in the spectra is most likely due to some residual methanol in the crystals. In an NMR sample where the solvent is DMSO, trace amounts of methanol will resonate at chemical shift of 3.13 ppm and 4.01 ppm.[27]

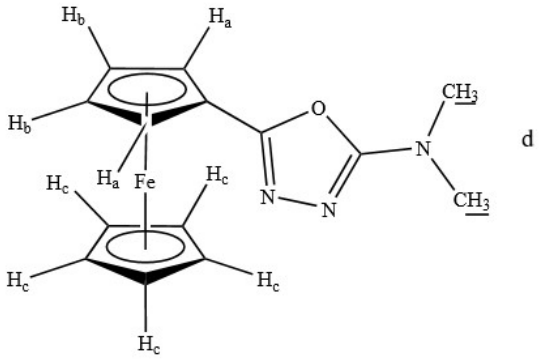


Figure 15. Structure of Compound **4**.

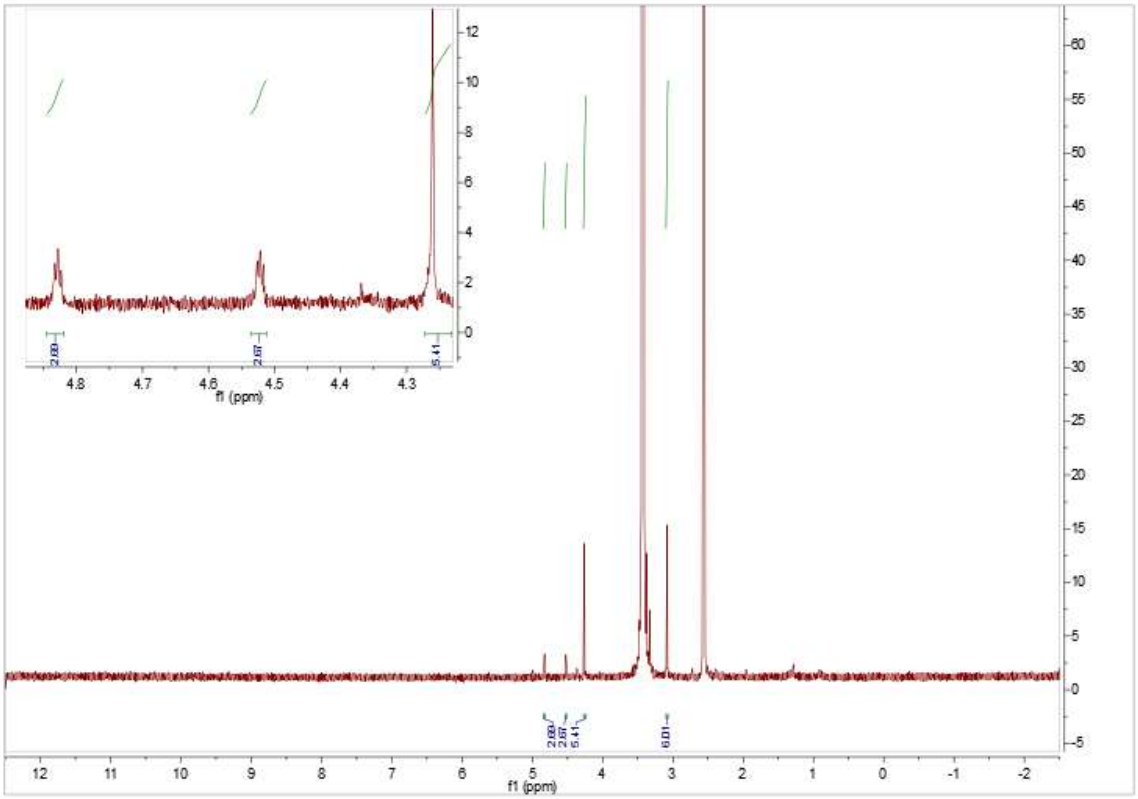


Figure 16. [1]H NMR of Compound **4** in DMSO-d6.

Table 3. Chemical shifts of reaction products from oxadiazole synthesis.

| | Assignment | Chemical Shift (ppm) | Integration | Theoretical Integration |
|---|---|---|---|---|
| **Compound 3** crude (Figure 13) | $H_a$ | 4.87 (t) | 2.00 | 2 |
| | $H_b$ | 4.37 (t) | 2.04 | 2 |
| | $H_c$ | 4.32 (s) | 4.90 | 5 |
| | $H_d$ | 9.71 (s) | 0.79 | 1 |
| | $H_e$ | 9.24 (s) | 0.79 | 1 |
| | $H_f$ | 3.23 (s) | 6.06 | 6 |
| **Compound 3** recrystallized (Figure 14) | $H_a$ | 4.87 (t) | 1.90 | 2 |
| | $H_b$ | 4.37 (t) | 1.80 | 2 |
| | $H_c$ | 4.32 (s) | 4.02 | 5 |
| | $H_d$ | 9.69 (s) | 1.00 | 1 |
| | $H_e$ | 9.24 (s) | 0.97 | 1 |
| | $H_f$ | 3.23 (s) | 5.40 | 6 |
| **Compound 4** Fc-oxadiazole (Figure 16) | $H_a$ | 4.83 (t) | 2.69 | 2 |
| | $H_b$ | 4.52 (t) | 2.67 | 2 |
| | $H_c$ | 4.26 (s) | 5.41 | 5 |
| | $H_d$ | 3.08 (s) | 6.01 | 6 |

The intramolecular cyclization of the purified Fc-thiosemicarbazide structure shown in Figure 12, yielding the final oxadiazole product shown in Figure 15, caused a drastic change in the number of peaks observed in the oxadiazole NMR shown in Figure 16. The amide protons, which resonated in the 9-10 ppm range of Figures 13 and 14 completely disappeared, and the six resonating -$CH_3$ protons shifted downfield from 5.40 ppm in the recrystallized Fc- thiosemicarbazide to 6.01 ppm in the Fc-oxadiazole product. The spacing between the $H_b$ and $H_c$ in the product also increased, due to the diminished electron-withdrawing effects of the carbonyl carbon the substituted cyclopentadienyl ring protons. As expected, the integrations of the resonating protons did not change drastically.

### 3.2 Lipophilicity (LogD) of Oxadiazole

Figures 17-22 show the UV-Vis scans of Compound **4** in 1-octanol (Figures 17-19) and aqueous phosphate buffer at pH 7.39 (Figures 20-22) at five different concentrations. The scans of the compound in each solution were run in triplicate.

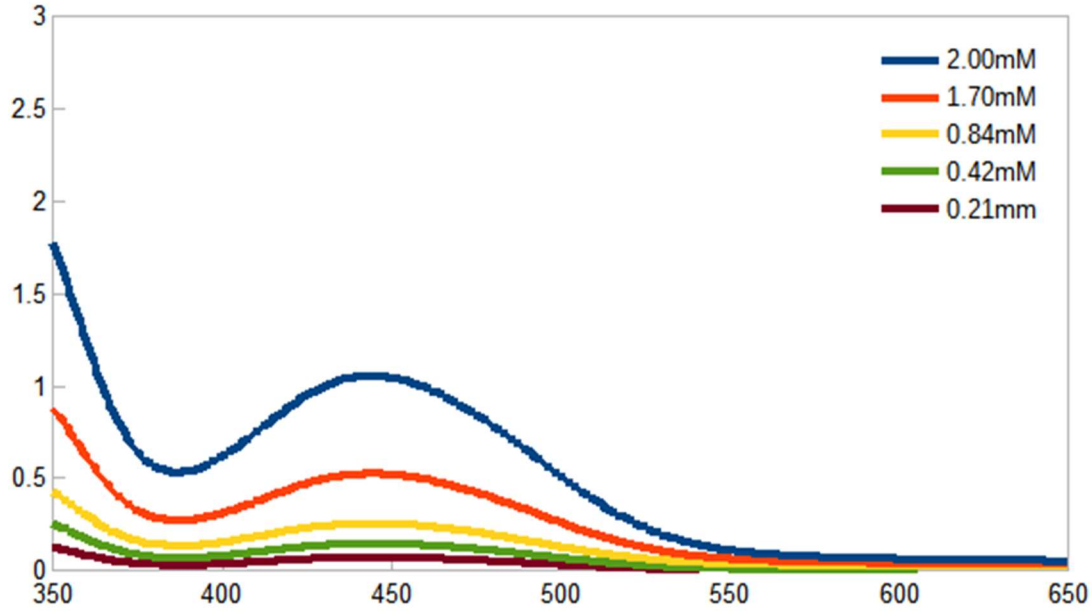


Figure 17. UV-Vis of Compound **4** in 1-octanol (Trial 1).

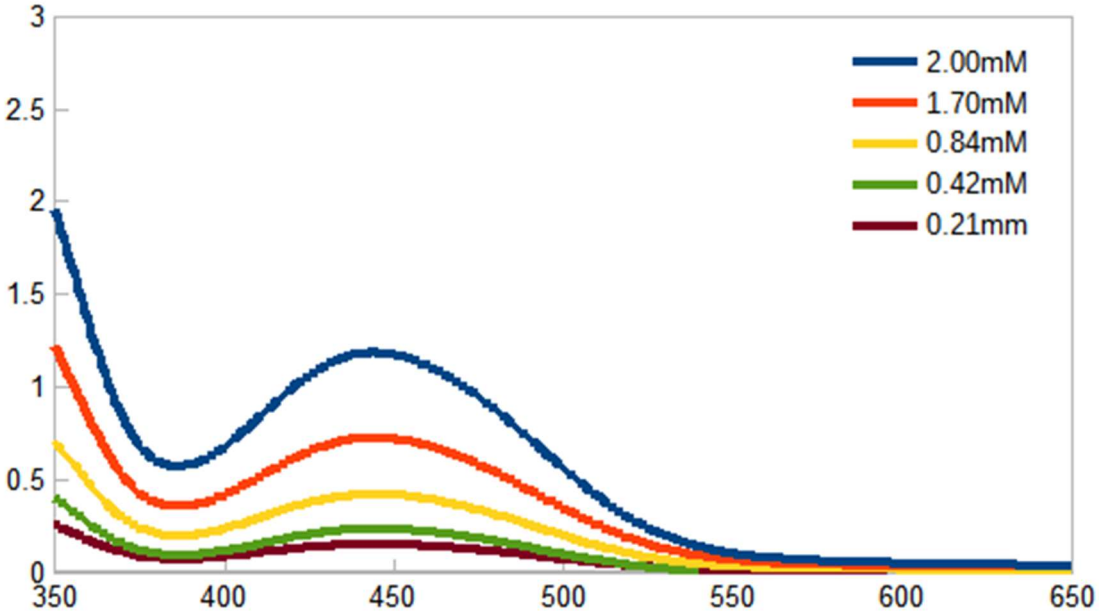


Figure 18. UV-Vis of Compound **4** in 1-octanol (Trial 2)

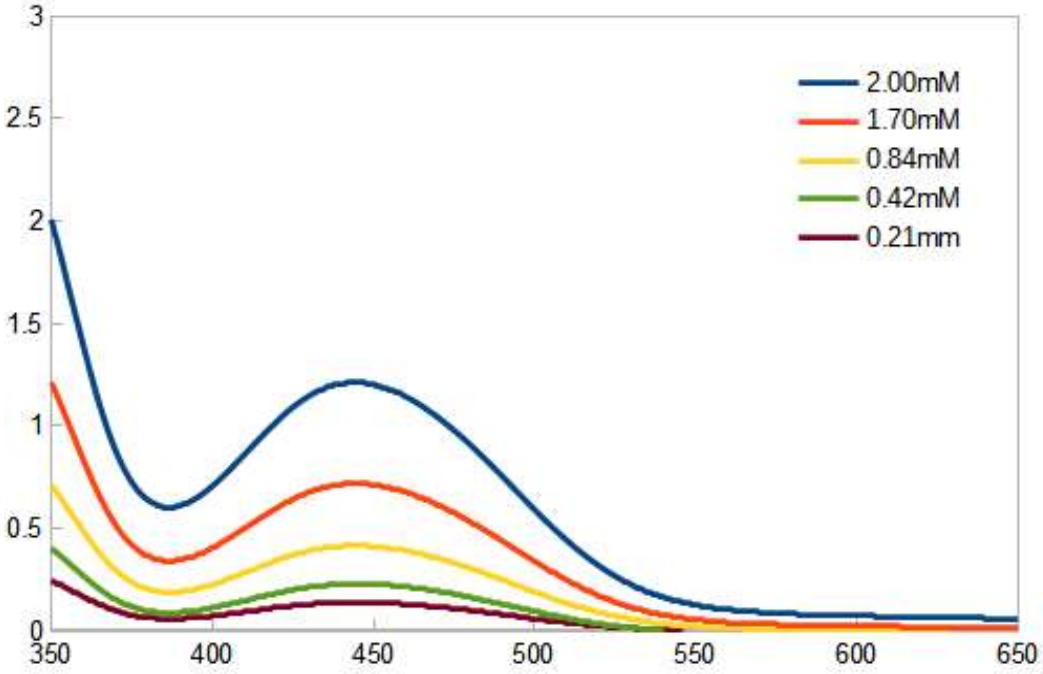


Figure 19. UV-Vis of Compound **4** in 1-octanol (Trial 3)

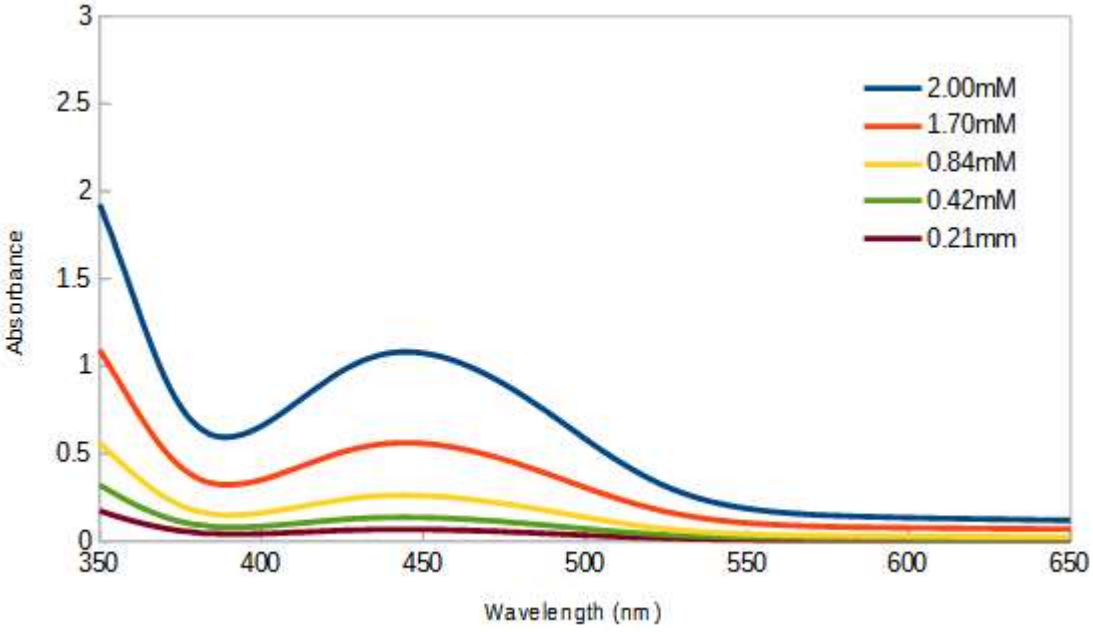


Figure 20. UV-Vis of Compound **4** in phosphate buffer (Trial 1)

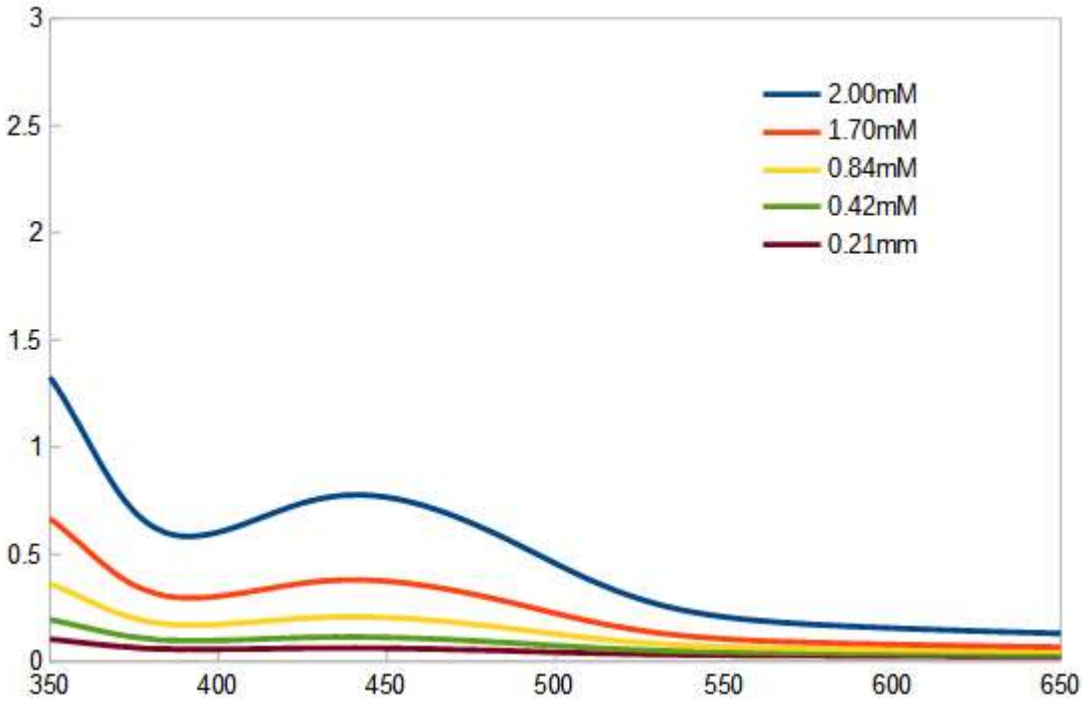


Figure 21. UV-Vis of Compound **4** in phosphate buffer (Trial 2)

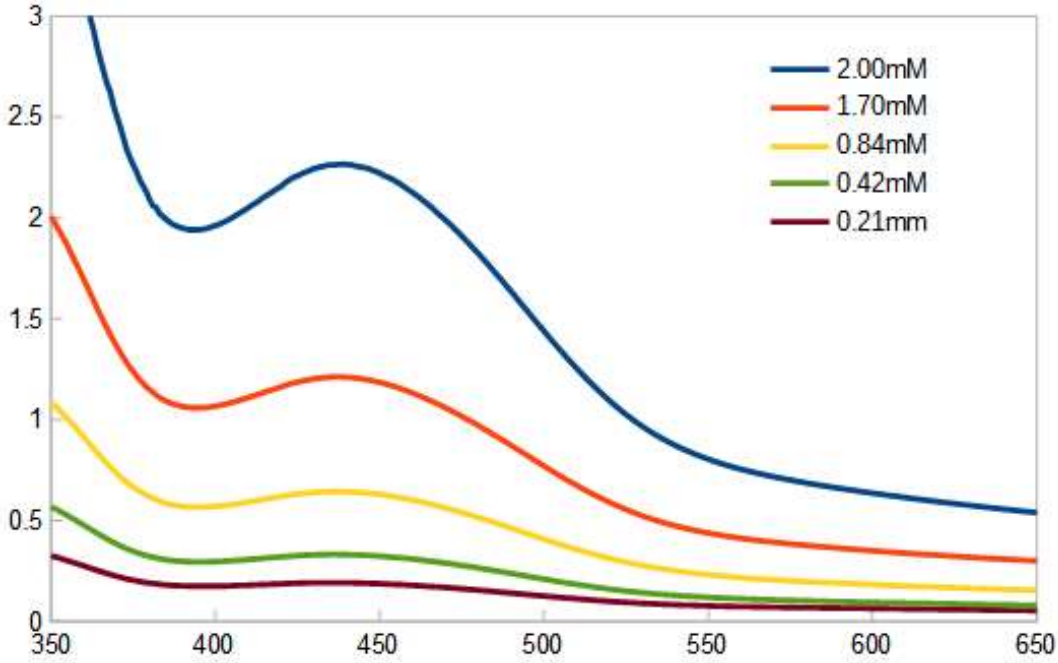


Figure 22. UV-Vis of Compound **4** in phosphate buffer (Trial 3)

The maximum absorbance in each of the six scans was found to be approximately 444 nm. The absorbances at 444 nm in each scan are shown in Table 4. From that information, calibration curves for the five concentrations in each phase were constructed and shown in Figures 23 and 24. The Y error bars on the graphs represent the standard deviation of the absorbances among the three trials. Since the spectrometer was blanked twice before each scan was taken (once with an air blank and once with the stock solution without analyte), and because Beer's Law assumes that a solution with no dissolved analyte will have 100% transmittance (i.e., no absorbance), the trendlines for the calibration curves were forced through the origin.

The Beer-Lambert Law is a commonly-used equation in UV-Visible spectroscopy which relates the absorbance of a compound with its molar concentration, the path length of the cuvette, and the extinction coefficient of that compound in a particular solvent. The equation for absorbance is written as:

$$A = \epsilon bc$$

where $A$ is the absorbance of the compound at a particular wavelength, $b$ is the path length of the cuvette (in cm), and $c$ is the concentration of the solution (in M). The extinction coefficient, ε, also known as molar absorptivity, is a characteristic of a compound at a specific wavelength in a specific solvent. Its value corresponds to the allowed-ness of the electronic transitions that the compound undergoes in the presence of UV radiation. Pure ferrocene, which absorbs at approximately 440 nm, undergoes a d to d electron transition.[28] In an organic solvent such as cyclohexane, this results in a molar absorptivity of 96 $M^{-1}cm^{-1}$.[29]

According to this law, the equation of the line of best fit obtained from a calibration curve can be used to determine the extinction coefficient of a compound.

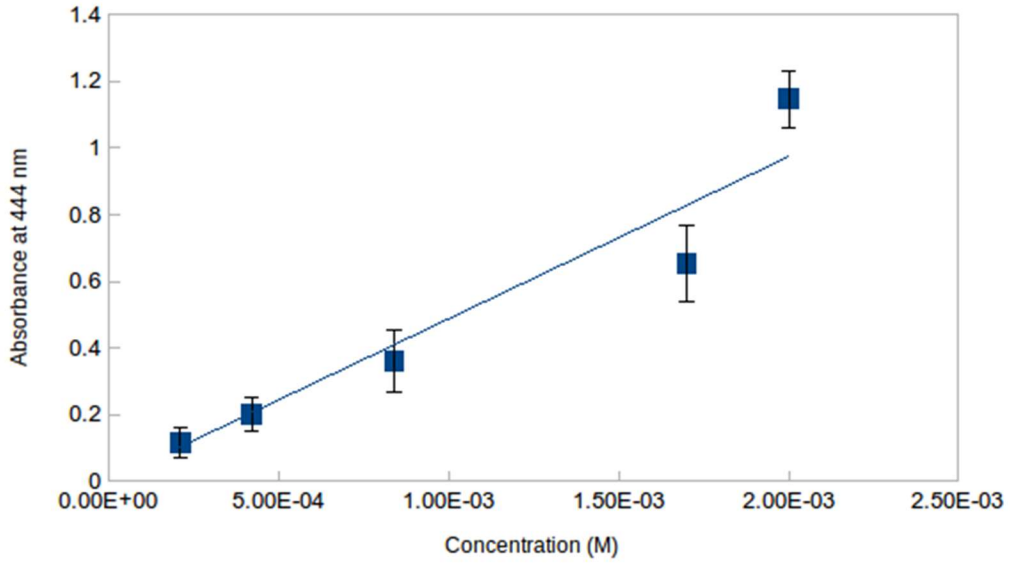


Figure 23. Calibration curve of Compound **4** in 1-octanol.
Trendline: y=488.625x ($R^2$ = 0.967)

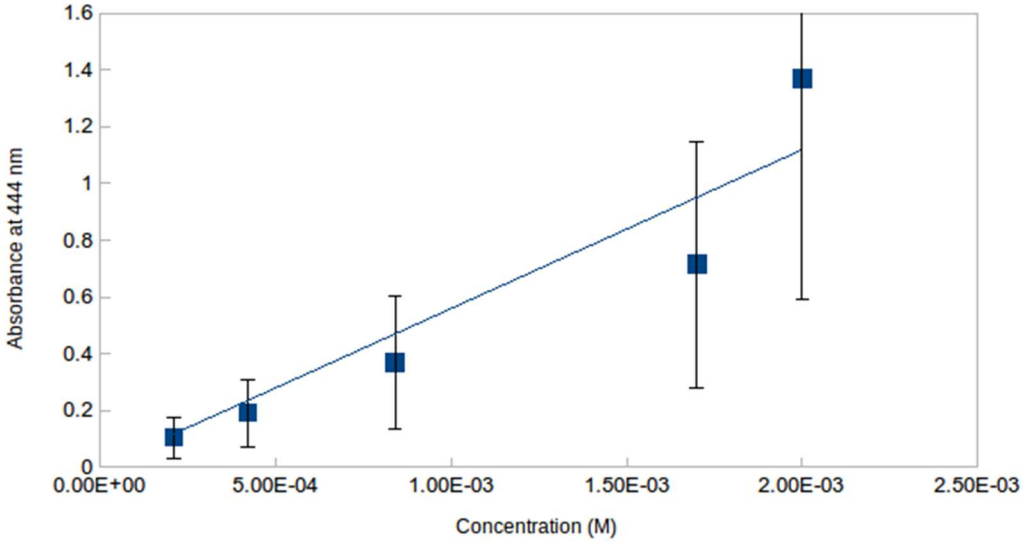


Figure 24. Calibration curve of Compound **4** in phosphate buffer
Trendline: y=558.945x ($R^2$ = 0.949)

Table 4. UV-Vis Absorbances and Concentrations at 444 nm.

| | **Concentration (M)** | **Trial 1 Abs.** | **Trial 2 Abs.** | **Trial 3 Abs.** | **Average Abs.** | **S.D.** |
|---|---|---|---|---|---|---|
| 1-octanol | $2.00 \times 10^{-3}$ | 1.053 | 1.181 | 1.211 | 1.148 | 0.086 |
| | $1.70 \times 10^{-3}$ | 0.520 | 0.723 | 0.717 | 0.654 | 0.115 |
| | $8.40 \times 10^{-4}$ | 0.251 | 0.417 | 0.414 | 0.361 | 0.095 |
| | $4.20 \times 10^{-4}$ | 0.142 | 0.229 | 0.229 | 0.200 | 0.050 |
| | $2.10 \times 10^{-4}$ | 0.066 | 0.147 | 0.134 | 0.117 | 0.044 |
| Phosphate buffer | $2.00 \times 10^{-3}$ | 1.082 | 0.775 | 2.251 | 1.370 | 0.779 |
| | $1.70 \times 10^{-3}$ | 0.562 | 0.379 | 1.204 | 0.715 | 0.433 |
| | $8.40 \times 10^{-4}$ | 0.262 | 0.206 | 0.639 | 0.370 | 0.235 |
| | $4.20 \times 10^{-4}$ | 0.136 | 0.112 | 0.329 | 0.193 | 0.119 |
| | $2.10 \times 10^{-4}$ | 0.067 | 0.061 | 0.190 | 0.106 | 0.073 |

The results of the modified shake-flask procedure are shown below in Figure 25.

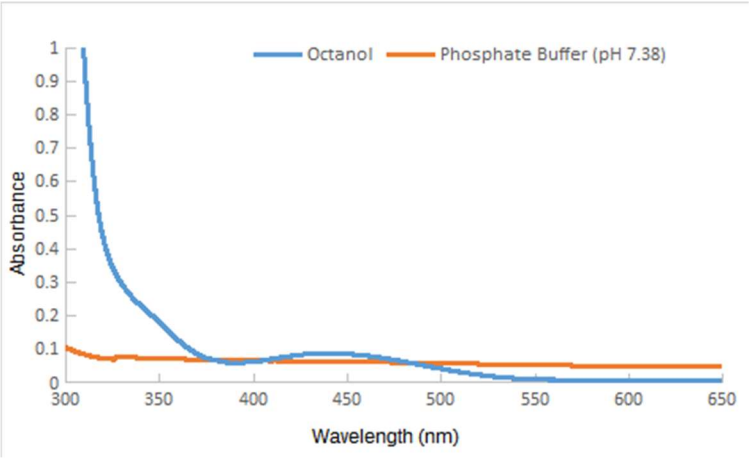


Figure 25. UV-Vis of organic and aqueous partitioning of Compound **4** ($\lambda_{max}$ = 441 nm)

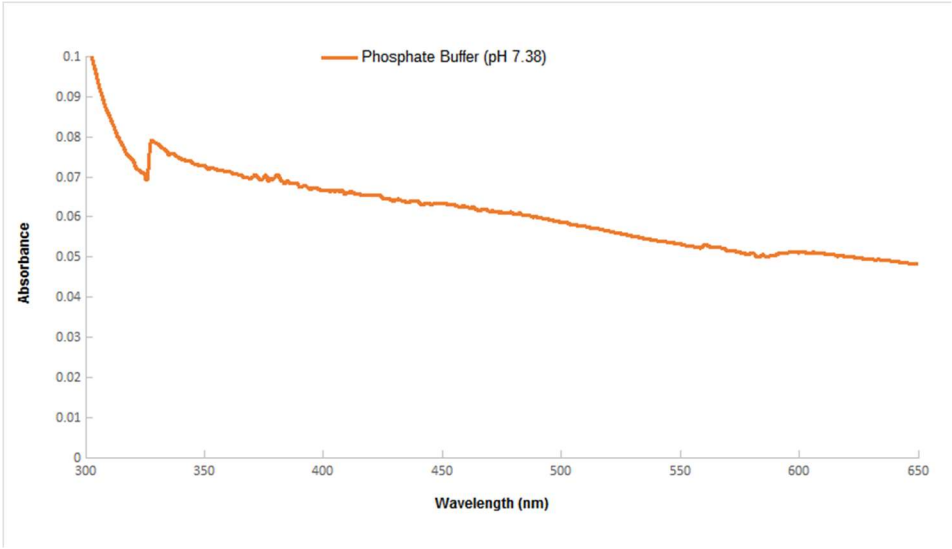


Figure 26. UV-Vis of the aqueous layer following partitioning.

Closer inspection of Figure 25 reveals the limited partitioning of Compound **4** in the aqueous layer compared with the organic layer. A calculation to estimate the number of moles in the organic phase was performed using the absorbance obtained at 444 nm in Figure 25 and the extinction coefficient calculated using data from Figure 23. This calculation resulted in an estimated 0.018 mmol of Compound **4** dissolved in the organic layer at the time of analysis. Considering that a total amount of 0.012 mmol of **4** were used for the partitioning in the experiment, we can be fairly certain that almost all of the compound has been partitioned into the organic layer. Inspection of Figure 26 confirms this observation, since there appears to be no appreciable absorbance at 444 nm. Any discrepancies between this calculated amount and the amount put into the system initially can be attributed to errors in the determination of the extinction coefficient.

Additionally, further analysis of the plot showing just the aqueous layer (shown in Figure 26) can be used to calculated a minimum LogD value for Compound **4**. Inspection of the small peak appearing at approximately 450 nm yields a corrected absorbance of

0.00205, and a noise level of approximately 0.00083, resulting in a signal-to-noise ratio of about 2.5. We can bracket the minimum LogD value through an estimate of the limit of detection, which is given by a signal-to-noise ratio of the spectrum multiplied by 3.[30] This results in a minimum absorbance value in the aqueous phase of 0.00615. Inserting this minimum absorbance value into Beer's Law yields the following concentration:

$$0.00615 = (559 M^{-1} cm^{-1})(1 cm)(c)$$

$$c = \frac{0.00615}{559 M^{-1} cm^{-1}}$$

$$C_{aqueous} = 1.1 \times 10^{-5}$$

Likewise, the concentration in the organic layer can be calculated as:

$$0.089 = (488.652 M^{-1} cm^{-1})(1 cm)(C)$$

$$C = \frac{0.089}{488.652 M^{-1} cm^{-1})(1 cm)}$$

$$C_{octanol} = 1.8 \times 10^{-4} M$$

Now that these concentrations are known, a lower limit on the LogD value can be estimated by:

$$LogD = log\left(\frac{1.8 \times 10^{-4}}{1.1 \times 10^{-5}}\right)$$

$$LogD = 1.21$$

This calculated LogD value at the detection limit of the compound in the aqueous layer means that, at a minimum, we can expect this compound to have a LogD value of 1.21. Enhanced methods of detection which are better suited to detect small concentrations (HPLC or UPLC), or by replication of the experiment with a larger initial quantity of analyte would yield a value close to or even higher than the one calculated here. Furthermore, using a mechanical shaker for a period of 24 hours of longer might demonstrate different results from the ones obtained here in which the sample was shaken by hand or agitated using a centrifuge. However, based on this calculation and an observation of the partitioning, we can conclude that Compound **4** is preferentially partitioned into the octanol layer. According to the information given in Table 1, compounds with a high LogD value (those which are more lipophilic) will demonstrate low blood solubility and poor metabolic stability owing to gastrointestinal permeability. Future synthetic attempts, therefore, should be directed towards creating compounds with more polar or charged groups.

### 3.3 Attempted Synthesis of 1-ferrocenoyl-4-phenylthiosemicarbazide via HBTU Coupling

Figures 27 and 28 show the structure and $^{1}H$ NMR, respectively, of Compound **5.** The starting material was dissolved in deuterated DMSO, so the peaks at 2.5 ppm and 3.3 ppm in the NMR reflect solvent and water, respectively. The three phenyl proton peaks can be seen in the NMR in the 7-8 ppm range, and have integrations values similar to the 2:2:1 ratio that was expected. While the NMR displays a broad singlet around 4.8 ppm which would be characteristic of an -NH group, there appears to be a much sharper singlet around 9.1 ppm and an additional, low-intensity peak just upfield at 9.6 ppm. Because of its proximity to lower electronegativity groups such as the C=S bond and the phenyl group, $H_c$ was assigned as the most upfield peak, and the $H_a$ protons were assigned as the sharp singlet at 9.1 ppm.

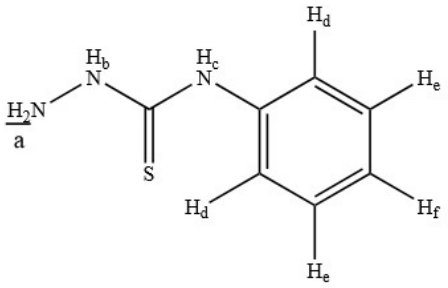


Figure 27. Structure of Compound **5**.

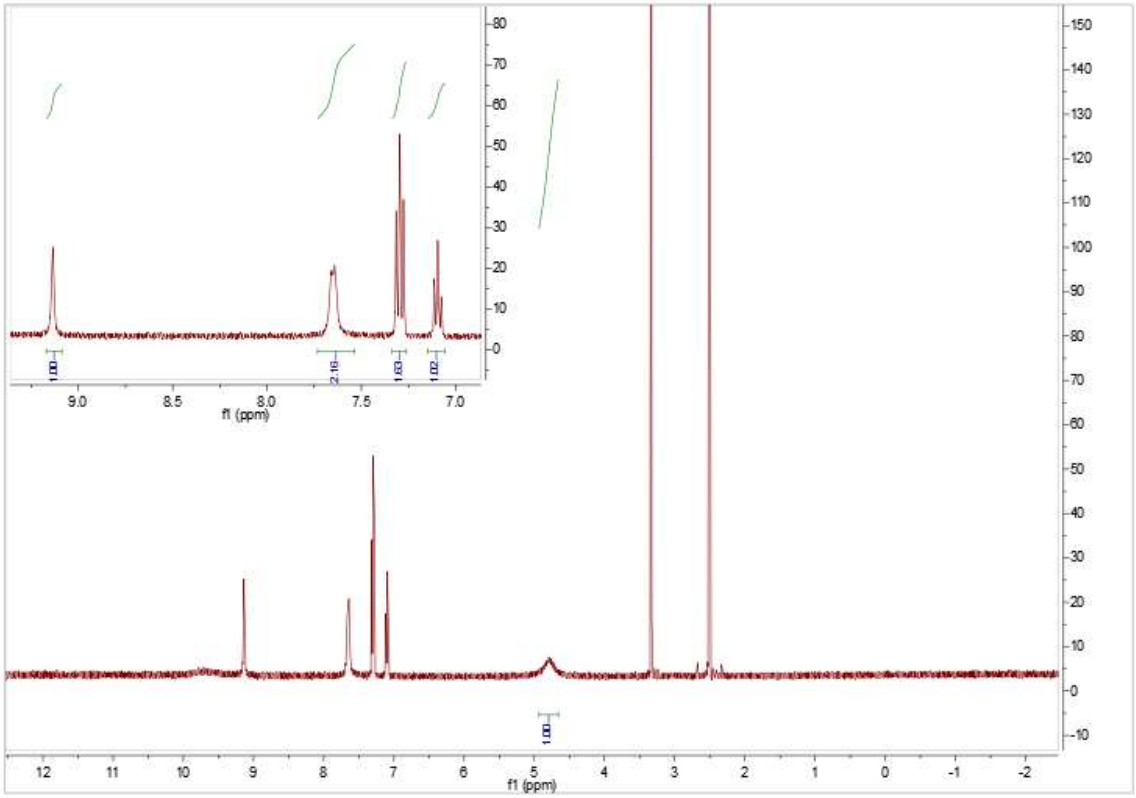


Figure 28. [1]H NMR of Compound **5** in DMSO-d6.

Based upon similarities between the initial structures of the starting materials and the mechanism of amide coupling employed by HBTU, the product structure of a reaction between Fc-monocarboxylic acid and 4-phenyl thiosemicarbazide was predicted to have a structure similar to the one shown in Figure 29. Figures 30-32 are the results of a first attempt at synthesizing and purifying this new compound through recrystallization.

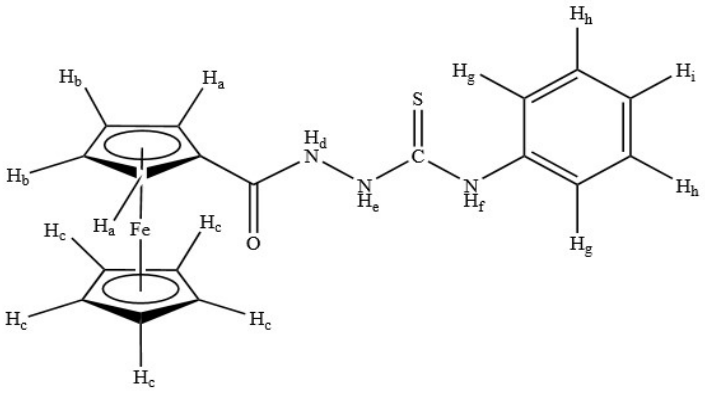


Figure 29. Attempted product of reaction between 4-phenylthiosemicarbazide and ferrocenemonocarboxylic acid (Compound **6**).

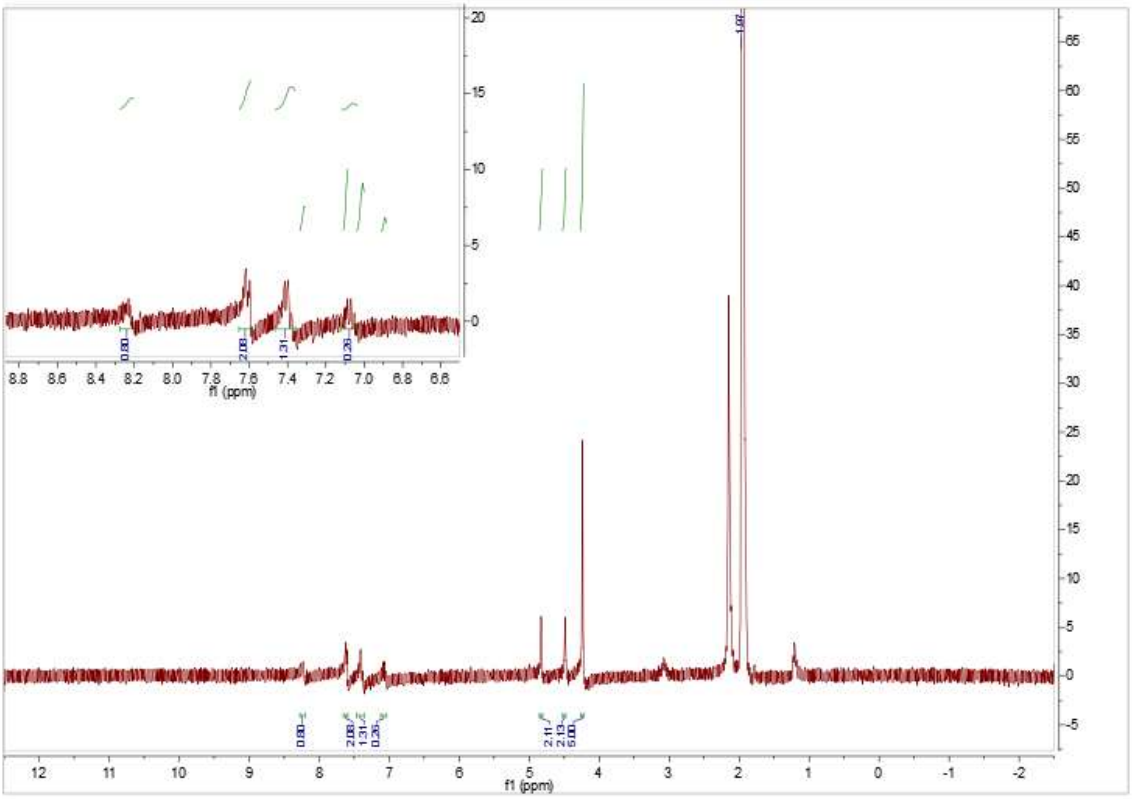


Figure 30. $^{1}$H NMR of crude Compound **6** in d-Acetonitrile.

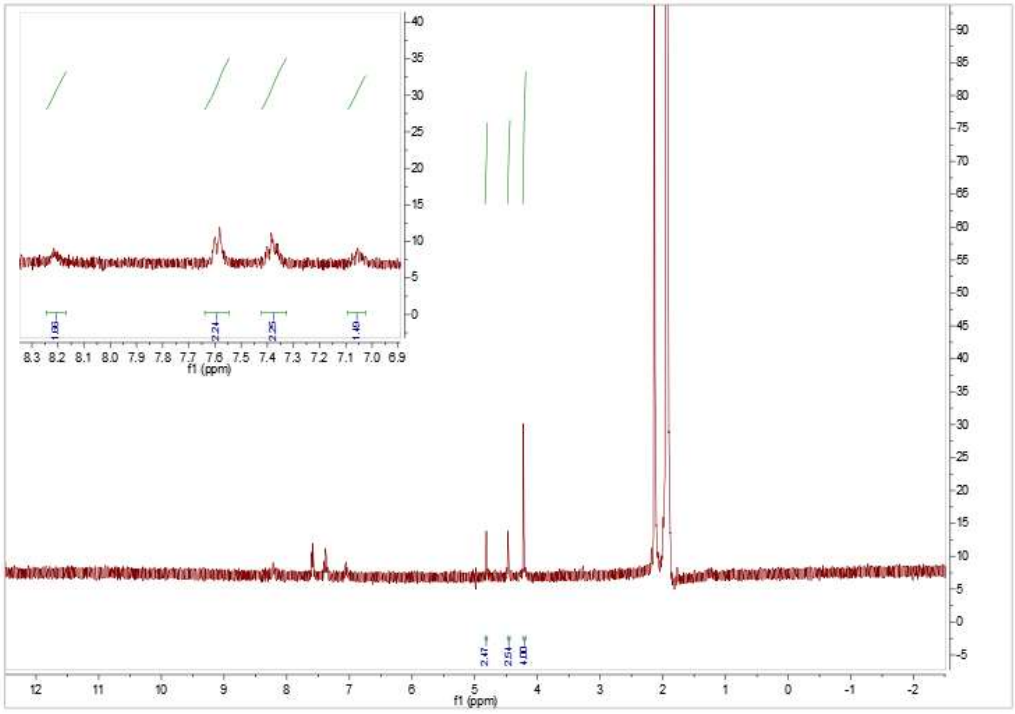


Figure 31. $^{1}$H NMR of Compound **6** in d-acetonitrile after recrystallization in methanol

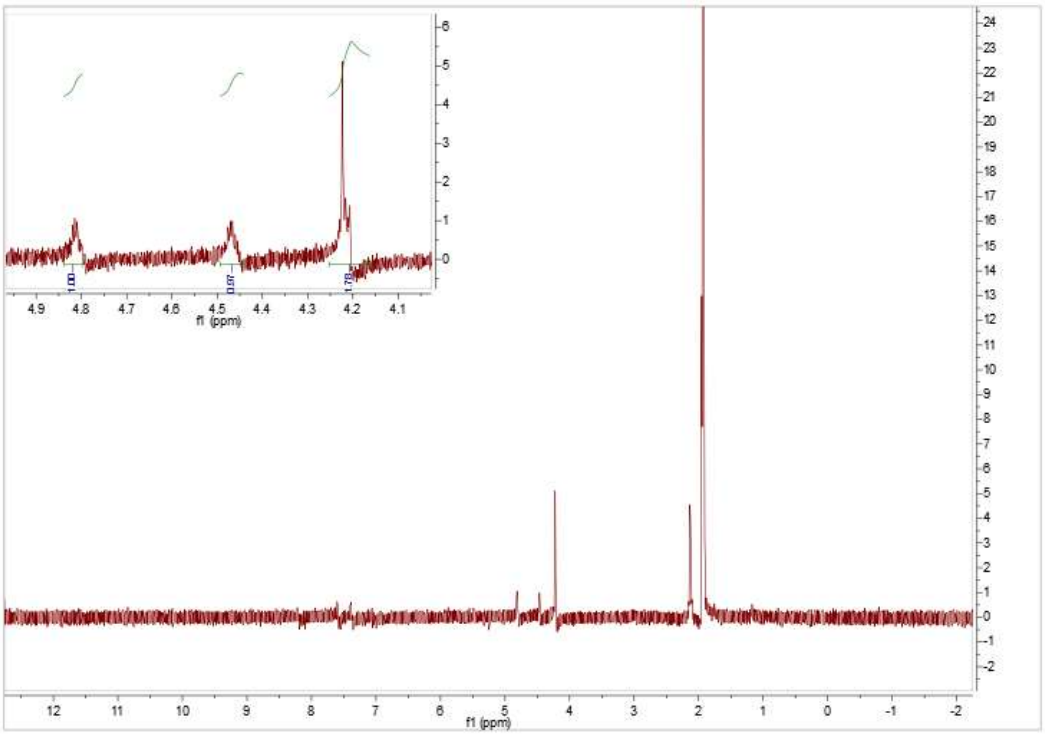


Figure 32. $^{1}$H NMR of Compound **6** after the second methanol recrystallization in d-acetonitrile

The peaks present in the sample of the crude product (Figure 30) demonstrate that the desired product might have actually been synthesized. The three characteristic peaks of a mono-substituted ferrocene are present in the 4-5 ppm range, all showing integration values similar to the 5:2:2 ratio that was expected. Similarly, the NMR of the crude product also showed the three peaks in the 7-8 ppm which closely resembled the positions of the three aromatic protons shown in the starting material. Additionally, the disappearance of at least one of the -NH peaks indicates that the amide coupling may have occurred as expected. The difficulty associated with analysis of the crude product is, since the yield was so low, the resolution of the peaks and the low signal-to-noise ratio made it difficult to discern the multiplicity of the peaks, as well as obtain accurate integrations. This challenge only increased when attempting to analyze the NMR of the first and second recrystallizations of the crude product in NMR. As seen in the resulting spectra in Figures 31 and 32, the signal-to-noise ratio of the peaks decreased so dramatically such that, after the second recrystallization, the none of the integrations or multiplicities of the aromatic protons in NMR could be obtained. Increasing the number of transients run by the NMR did little to improve the resolution of the peaks or the signal to noise ratio. Both of the spectra showing the product after each successive recrystallization were acquired with nt=100, which means that in order to see any significant improvement, the number of scans might have to be increased to 1000 or higher. The continued persistence of those phenyl peaks and the three ferrocene peaks through multiple recrystallizations indicates that the product was likely present in small quantities. Table 5 gives a summary of the chemical shifts of the thiosemicarbazide starting material and the products, both crude and recrystallized.

Table 5. Chemical shifts of Fc-phenylthiosemicarbazide synthesis reactants and products.

| | Assignment | Chemical Shift (ppm) | Integration | Theoretical Integration |
|---|---|---|---|---|
| **Compound 5** (Figure 28) | $H_a$ | 9.13 (bs) | 1 | 2 |
| | $H_b$ | 9.68 (s) | 1 | 1 |
| | $H_c$ | 4.79 (bs) | 0.06 | 1 |
| | $H_d$ | 7.63 (d) | 2.16 | 2 |
| | $H_e$ | 7.30 (t) | 1.83 | 2 |
| | $H_f$ | 7.09 (t) | 1.02 | 1 |
| **Compound 6**; crude. (Figure 30) | $H_a$ | 4.24 (s) | 5.00 | 5 |
| | $H_b$ | 4.49 (t) | 2.13 | 2 |
| | $H_c$ | 4.83 (t) | 2.11 | 2 |
| | $H_e$ | 8.27 | 0.80 | 1 |
| | $H_g$ | 7.62 | 2.08 | 2 |
| | $H_h$ | 7.34 | 1.31 | 2 |
| | $H_i$ | 7.06 | 0.28 | 1 |
| **Compound 6**; recryst. (Figure 31) | $H_a$ | 4.2 (d) | 4.00 | 5 |
| | $H_b$ | 4.48 (t) | 2.54 | 2 |
| | $H_c$ | 4.82 (t) | 2.47 | 2 |
| | $H_e$ | 8.27 | 1.86 | 1 |

| | | | | |
|---|---|---|---|---|
| | $H_g$ | 7.58 | 2.24 | 2 |
| | $H_h$ | 7.39 | 2.25 | 2 |
| | $H_i$ | 7.06 | 1.49 | 1 |
| **Compound 6**; second recryst. (Figure 32) | $H_a$ | 4.2 (s) | 4.81 | 5 |
| | $H_b$ | 4.48 (t) | 1.89 | 2 |
| | $H_c$ | 4.82 (t) | 2.29 | 2 |

This particular trial of the synthesis, however, turned out to be the only attempt with results resembling the predicted structure of the final product. Following the first attempt at synthesis, the results of which are shown here, further attempts at synthesis yielded no compounds or spectra which remotely resembled the attempted product. Multiple trials were run in which the acetonitrile was evaporated to dryness immediately following the 24-hour stir period, followed by washes with ethyl acetate, ether, and hexane. This resulted in NMR spectra which were missing either the ferrocene peaks, the phenyl peaks, or both. It was proposed, at this point, that perhaps the HBTU was interacting with the aromatic protons of the thiosemicarbazide or one or more of the amine protons. These interactions would not have been witnessed in the coupling between the Compound **1** and Compound **2** because of the absence of such protons. In order to keep working with this promising starting material, an alternative method of synthesis would need to be determined that did not rely on a coupling agent.

### 3.4 Attempted Synthesis of Compound 6 using a Carbonyl Chloride Intermediate

The structure of ferrocene carbonyl chloride, **7**, is shown in Figure 33. The spectrum shown in Figure 34 is of the crude red oil obtained from the Schlenk flask.

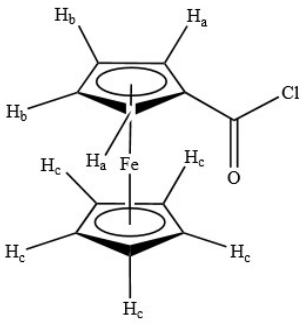


Figure 33. Structure of Compound **7**.

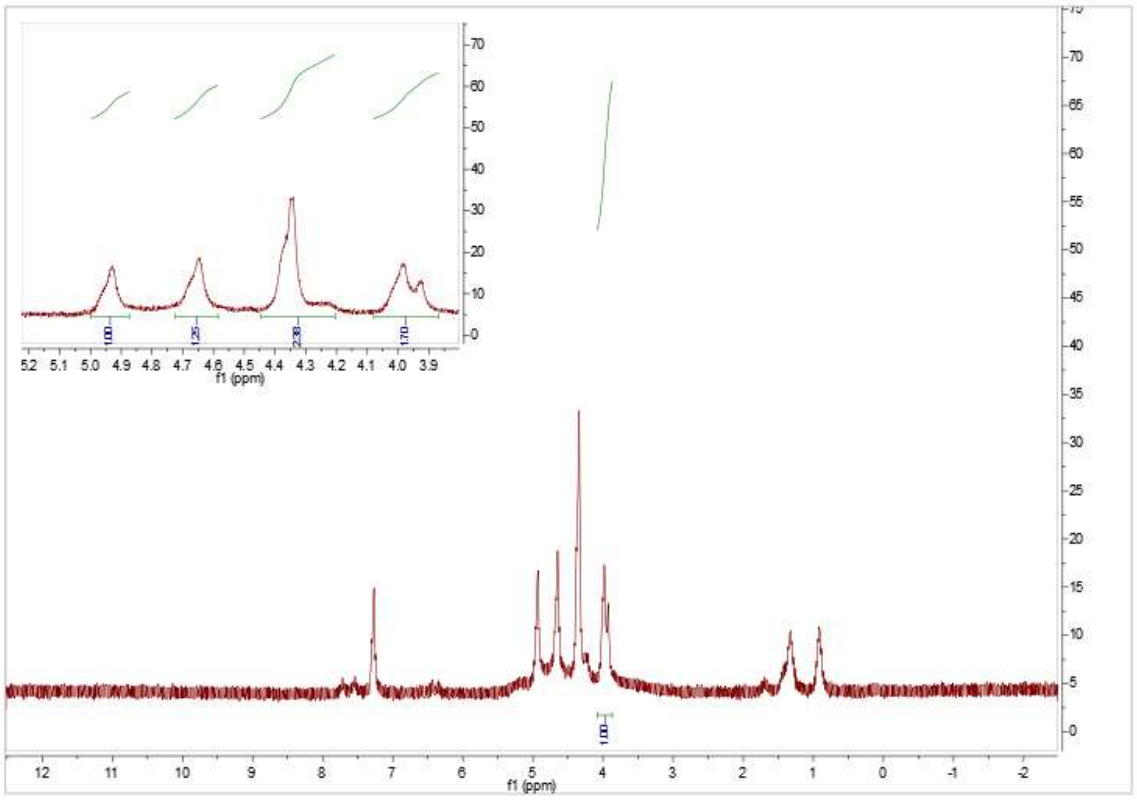


Figure 34. $^{1}$H NMR of Compound **7** in chloroform-d after washes with pet. ether and pentane.

The large singlet at 7.26 ppm can be attributed to the chloroform-d in which the sample was run. The two small singlets appearing from 7.5-8 ppm are most likely remnants of residual pyridine, which was used as a base catalyst during the reflux period. The two upfield singlets in the 0.5-1.5 ppm range are most likely due to trace amounts of pentane, which was used during the washing process and displays singlets at 0.88 and 1.27 ppm in chloroform. Furthermore, the four peaks within the 4-5 ppm range give some indication that a monosubstituted ferrocene is still present in the sample.

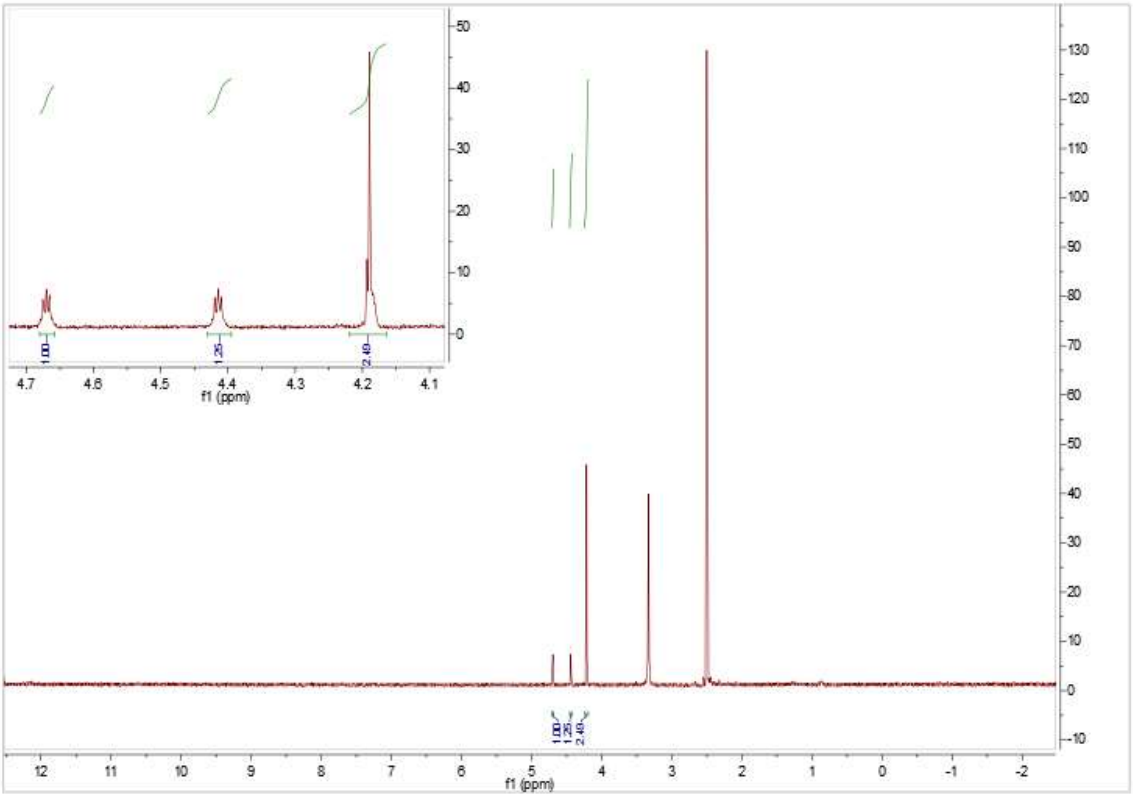


Figure 35. $^{1}$H NMR of Compound **7** in DMSO-d6 after recrystallization in chloroform-d.

Figure 35 shows the spectrum of a small sample of Compound **7** which was obtained from the test tube of the original NMR sample several days following its preparation. All of the chloroform-d had evaporated from the test tube, leaving behind a fine, grayish-brown powder in the bottom of the tube and a series of long, orange needles

which had grown up the side of the flask. NMR of a few of these crystals in DMSO revealed an incredibly clean spectrum, with three peaks in the 4-5 ppm range which integrated almost exactly to the values expected for the ferrocene compound. The split peak at 4.2 ppm, which ideally should have been a singlet, is the only indication that there are any impurities in this spectra. Furthermore, the chemical shifts of those three peaks in Figure 35 allow this product to be distinguished from Compound **1**'s spectrum shown in Figure 7. The three Cp proton peaks resonate at 4.3, 4.5, and 4.7 ppm in the carboxylic acid starting material, and shift to 4.2, 4.5, and 4.6 ppm in the spectrum of the carbonyl chloride. However, the extremely small size of recovered pure crystals (0.002 grams) made it impossible to use this purified product for reaction with Compound **5**, so the remnants of the red oil were used instead. Figures 36-38 show the crude product of this reaction, the product following the first recrystallization in methanol, and the product following the second recrystallization in methanol, respectively.

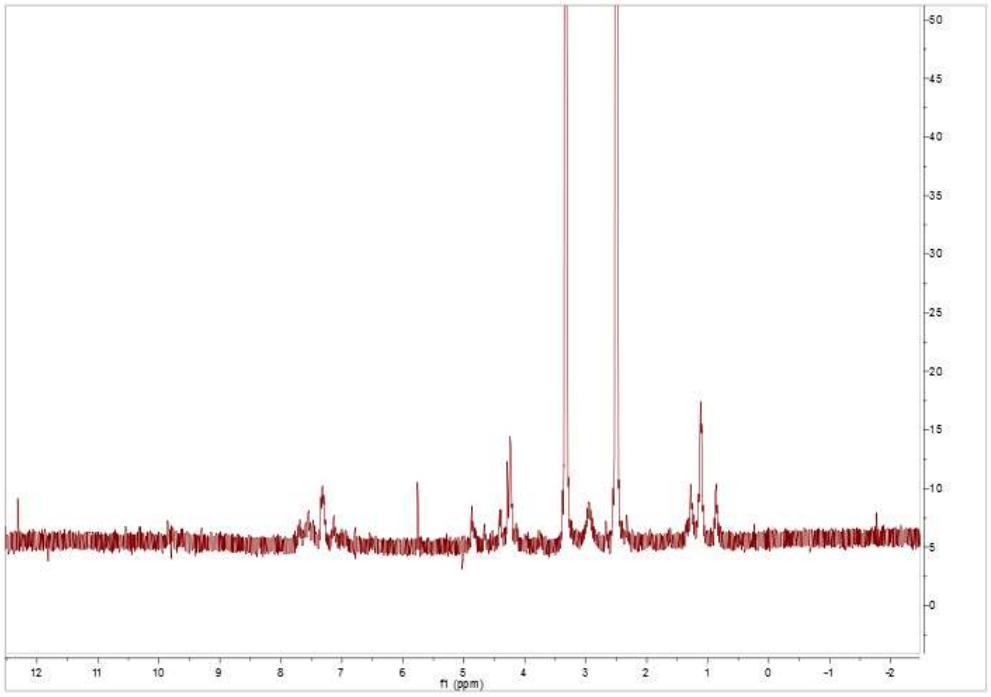


Figure 36. $^{1}$H NMR of crude product from carbonyl chloride - phenylthiosemicarbazide synthesis in DMSO-d6.

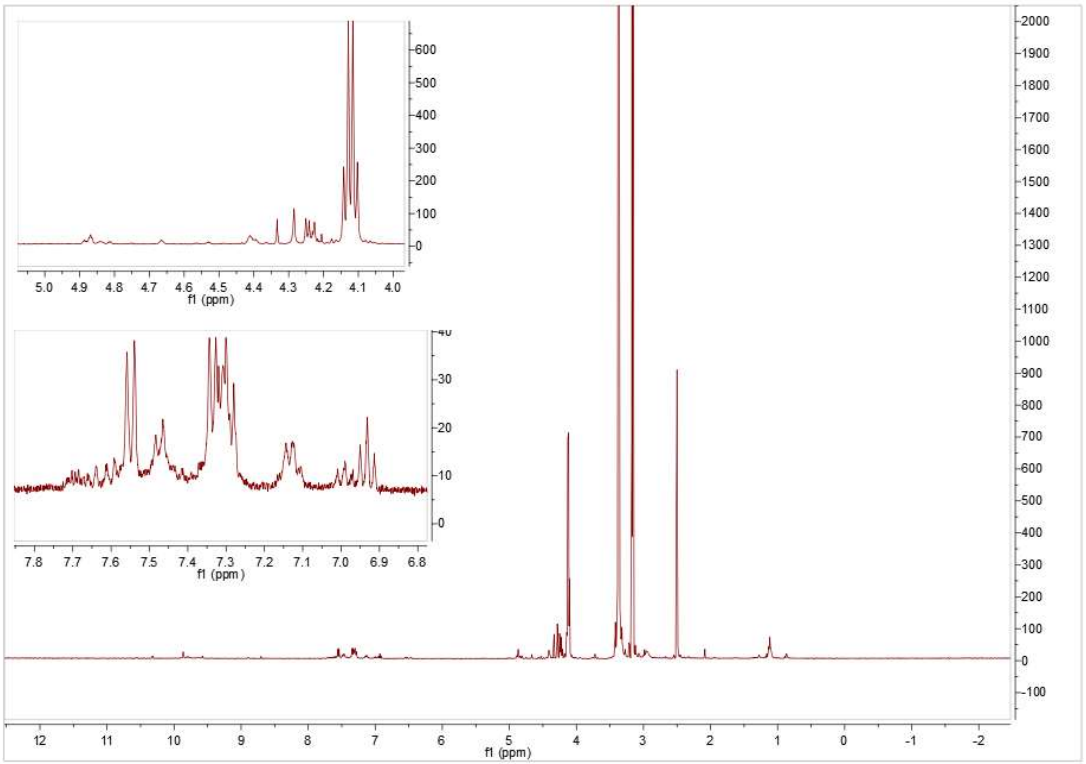


Figure 37. $^{1}$H NMR of first recrystallization product in DMSO-d6.

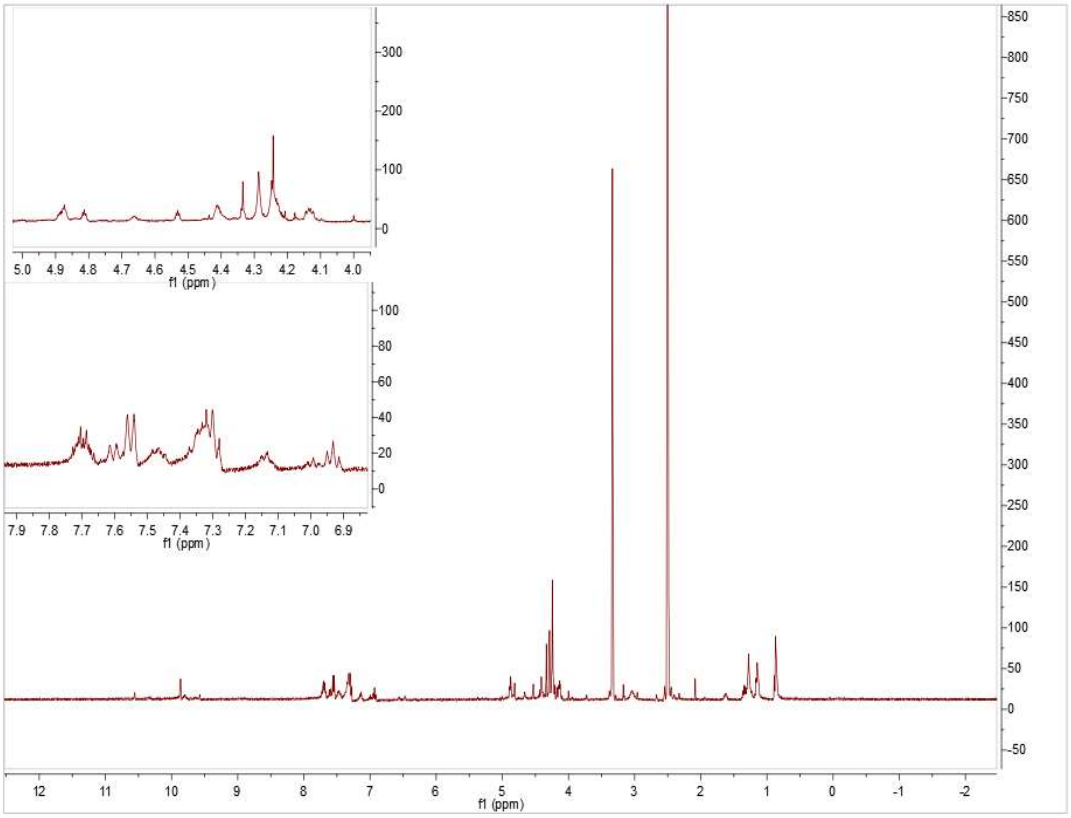

Figure 38. $^{1}$H NMR of second recrystallization product in DMSO-d6.

The resulting spectra from this synthesis, due to the large clusters of peaks and multiplets, don't allow any specific conclusions to be made about the exact structure of the product. All three spectra, do however, contain clusters of peaks in certain regions which can be useful in generalizing the structures of the product. The clusters of peaks in the 4-5 ppm range and the 7-8 ppm range are, as mentioned before, characteristic of the monosubstituted ferrocene and the aromatic protons on the phenyl thiosemicarbazide, respectively. Since the solvent was evaporated from the reaction mixture with a vacuum immediately following the 24-hour reaction period, the abundance of peaks in the 0.5-2 ppm range could be contributed by residual pentane (from the oil), petroleum ether, or both.

### 3.5 Attempted Synthesis of 1-ferrocenoyl-4-(3-nitrophenyl)-3-thiosemicarbazide

Figures 39-41 show the attempted synthesis of the product of Compound **1** acid with 4-(3-nitrophenyl)-3-thiosemicarbazide, **8**. The structure and NMR of the starting material are shown in Figures 39 and 40, respectively.

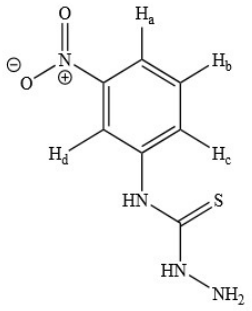


Figure 39. Structure of Compound **8**.

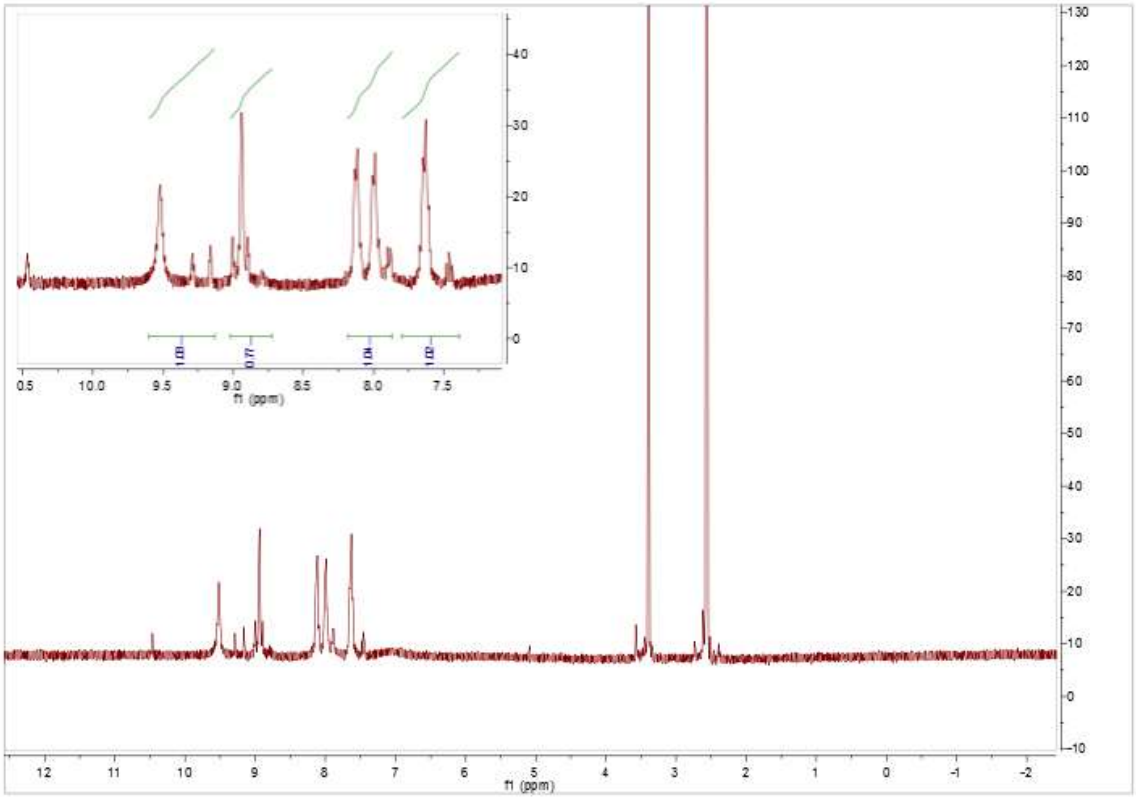


Figure 40. $^{1}$H NMR of Compound **8** in DMSO-d6.

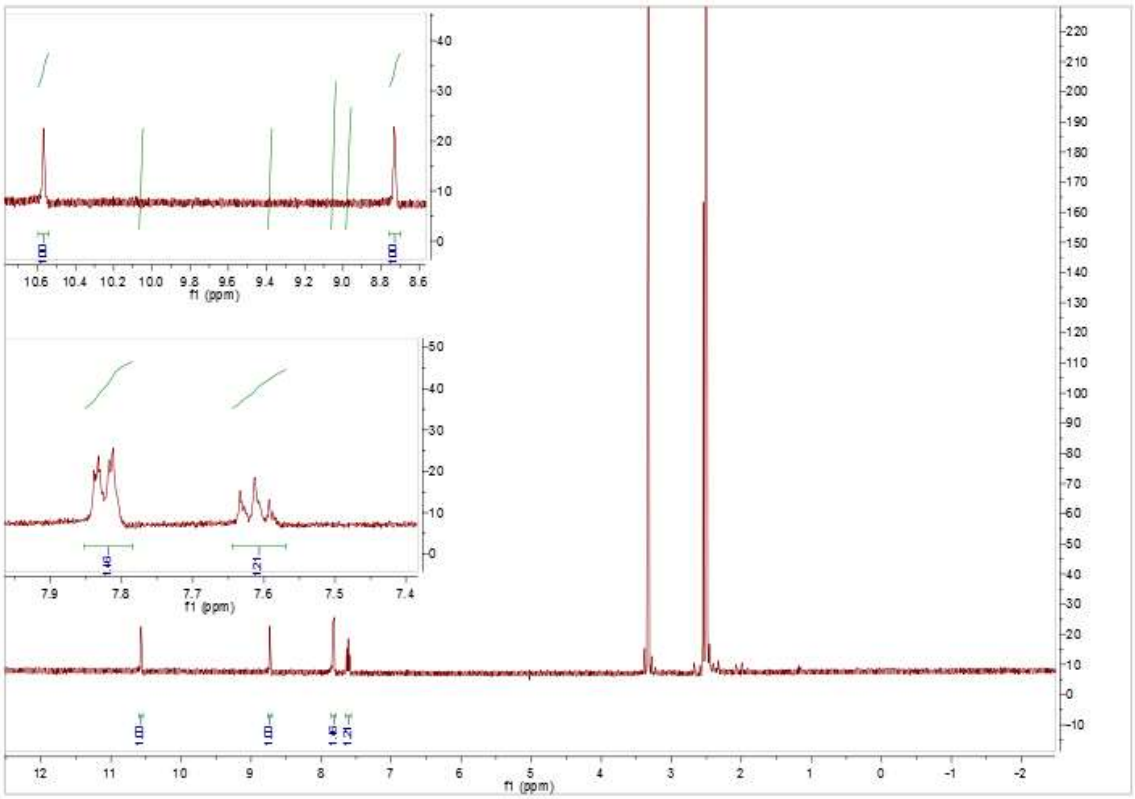


Figure 41. $^{1}$H NMR of crude Fc-nitrothiosemicarbazide product in DMSO-d6.

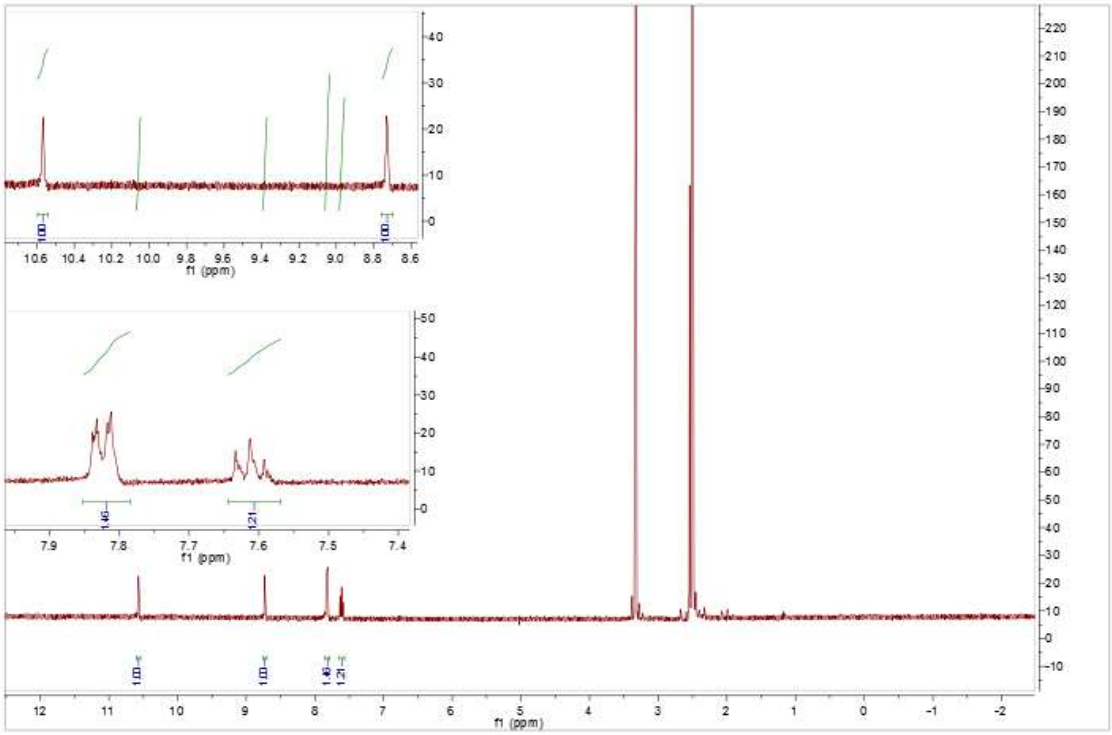


Figure 42. $^{1}$H NMR of product in DMSO-d6 recrystallized in methanol.

The resulting spectra of this synthesis clearly show that the final product isolated product contains no traces of ferrocene monocarboxylic acid. Since this reaction was accomplished using HBTU, it is likely that the same issues which plagued the attempted synthesis of Compound **6** are present here. The HBTU seems unable to have initiated the dehydration reaction between the amine on the thiosemicarbazide and the carboxylic acid of the ferrocene. Since Compound **1** is much more hydrophobic and therefore much more soluble in acetonitrile compared with the relatively polar Compound **8**, it is likely that the dark brown reaction liquid which was drawn off the flask and subsequently discarded contained the unreacted ferrocene. The subsequent washes with ethyl acetate, also a nonpolar solvent, probably removed all other traces of the monosubstituted ferrocene, which would account for why those peaks did not present themselves in the spectra of the product. Interestingly enough, the differences in the spectra between the starting material and the reaction products indicate that some chemistry was most likely worked on the aromatic protons of Compound **8**. Although the overall positions of the peaks do not change from the crude product to the recrystallized material, we instead see two singlets appear at approximately 8.7 and 10.5 ppm, and two other multiplets appear at 7.6 and 7.8 ppm.

# 4. CONCLUSIONS AND FUTURE WORK

This research describes attempts at synthesizing a variety of novel oxadiazole-containing compounds. The aqueous solubility of one such compound, N,N-dimethyl(5-ferrocenoyl-1,3,4,-oxadiazol-2-yl)amine, was determined using a modified shake-flask procedure, which employed UV-Vis spectroscopy to quantify the amount of compound in each phase of an organic and aqueous solvent system. The results of the partition between 1-octanol and an aqueous phosphate buffer resulted in a minimum estimated LogD value of 1.21, which indicates that this particular molecule could possibly demonstrate poor blood solubility and lower metabolic stability/high GI absorptivity. Furthermore, three other attempts were described here to derivatize ferrocene monocarboxylic acid with two aromatic thiosemicarbazides, 4-phenylthiosemicarbazide and 4-(3-nitrophenyl)-3-thiosemicarbazide. Two methods of synthesis employed HBTU as a coupling agent as a means of amide bond formation between the monocarboxylic acid and the amine of the thiosemicarbazide, but these attempts were faced with challenges with regards to reproducibility, or, in the case of the nitrothiosemicarbazide, apparent difficulties with selectivity of the HBTU in the presence of strong electron-withdrawing groups on the aromatic ring. In order to bypass the need for a coupling agent, an additional procedure was carried out which involved the conversion of ferrocene monocarboxylic acid into ferrocene carbonyl chloride through treatment with oxalyl chloride. The choice to create a carbonyl chloride yielded very positive results and, given enough time to continue purifying the final product, might actually be a more effective and simpler means of attaching a thiosemicarbazide onto the ferrocene.

Given additional time to complete this project, there are a number of additional steps which could be taken. Because of the success achieved using a carbonyl chloride intermediate, the products of these reactions could be further purified to achieve, potentially, any number of thiosemicarbazide structures. Once a method for the purification of these new structures could be identified, the structures could be reacted with mercury in a similar prep of the first oxadiazole, in order to see whether or not intramolecular cyclization will still occur in the presence of various other R groups on the thiosemicarbazide. If it is found that oxadiazole were, in fact, formed during this step, a determination of their LogD values, metabolic stability using a microsomal stability assay, and other *in vitro* tests could be used to further assess whether or not these new molecules possess any type of medicinal properties.

## BIBLIOGRAPHY


1. Supamon, M. Infrared Spectroscopy and Electrochemical Based Methods of Mercury (II) Detection via Reactions with Surface-Bound and Solution Ferrocenyl Acylthiosemicarbazide. University of Maine, 2014.
2. de Oliveira, C. S.; Lira, B. F.; Barbosa-Filho, J. M.; Lorenzo, J. G. F.; de Athayde-Filho, P. F., Synthetic approaches and pharmacological activity of 1,3,4-oxadiazoles: a review of the literature from 2000-2012. *Molecules (Basel, Switzerland)* 2012, *17* (9), 10192-10231.
3. Bostrom, J.; Hogner, A.; Llinas, A.; Wellner, E.; Plowright, A. T., Oxadiazoles in Medicinal Chemistry. *Journal of Medicinal Chemistry* 2012, *55* (5), 1817-1830.
4. Amarasinghe, K. K. D.; Maier, M. B.; Srivastava, A.; Gray, J. L., One-pot synthesis of 1,2,4-oxadiazoles from carboxylic acid esters and amidoximes using potassium carbonate. *Tetrahedron Letters* 2006, *47* (22), 3629-3631.
5. Zarghi, A.; Hajimahdi, Z., Substituted oxadiazoles: a patent review (2010-2012). *Expert Opinion on Therapeutic Patents* 2013, *23* (9), 1209-1232.
6. Perry, C. M., Raltegravir: a review of its use in the management of HIV-1 infection in children and adolescents. *Paediatric drugs 16* (1), 91-100.
7. Wei, C. Y.; Liu, Z. Y.; Zhang, D. W.; Mei, Y., DOCKING OF RALTEGRAVIR TO HIV-1 INTEGRASE STRUCTURE ENSEMBLE. *Journal of Theoretical & Computational Chemistry* 2010, *9* (6), 1053-1063.
8. Benet, L. Z.; Zia-Amirhosseini, P., Basic principles of pharmacokinetics. *Toxicologic Pathology* 1995, *23* (2), 115-123.
9. Beaumont, C., Human ADME Properties of Drug Molecules: a Plethora of Approaches. *British journal of clinical pharmacology*, n-a-n/a.
10. Rowe, P., Pharmacokinetics. Bookboon: 2012.
11. Ebbing; Gammon, General Chemistry. 6th ed.; Houghton Mifflin Company.: Boston, MA, 1999; pp 502-505.
12. Williams, H. D.; Trevaskis, N. L.; Charman, S. A.; Shanker, R. M.; Charman, W. N.; Pouton, C. W.; Porter, C. J. H., Strategies to address low drug solubility in discovery and development. *Pharmacological Reviews* 2013, *65* (1), 315-499.
13. Goldberg, K.; Groombridge, S.; Hudson, J.; Leach, A. G.; MacFaul, P. A.; Pickup, A.; Poultney, R.; Scott, J. S.; Svensson, P. H.; Sweeney, J., Oxadiazole isomers: all bioisosteres are not created equal. *Medchemcomm* 2012, *3* (5), 600-604.
14. Werner, H. H., At least 60 years of ferrocene: the discovery and rediscovery of the sandwich complexes. *Angewandte Chemie (International ed.)* 2012, *51* (25), 6052-6058.
15. Navarro, A. E.; Spinelli, N.; Moustrou, C.; Chaix, C.; Mandrand, B.; Brisset, H., Automated synthesis of new ferrocenyl-modified oligonucleotides: study of their properties in solution. *Nucleic Acids Research* 2004, *32* (17), 5310-5319.
16. Babin, V. N.; Belousov, Y. A.; Borisov, V. I.; Gumenyuk, V. V.; Nekrasov, Y. S., Ferrocenes as potential anticancer drugs. Facts and hypotheses. *Russian chemical bulletin 63* (11), 2405-2422.
17. Nesmeyan.An; Bogomolo.Lg; Andriano.Ig; Vilchevs.Vd; Kochetko.Ns, NEW COMPOUND (FERROCERONE) FOR TREATMENT OF IRON - DEFICIENT ANEMIA. *Khimiko-Farmatsevticheskii Zhurnal* 1972, *6* (4), 61-&.

18. Gasser, G., Organometallic Anticancer Compounds. *J. Med. Chem.* 2011, *54* (1), 3-25.
19. Gasser, G.; Metzler-Nolte, N., The potential of organometallic complexes in medicinal chemistry. *Current opinion in chemical biology 16* (1-2), 84-91.
20. Masimirembwa, C. M. B. U. T. B., Metabolic Stability for Drug Discovery and Development: Pharmacokinetic and Biochemical Challenges. *Clinical Pharmacokinetics* 2003, *42* (6), 515-528.
21. Scully, C. C. G.; Lau, Y. H.; Jensen, P.; Rutledge, P. J., Synthesis, electrochemistry and metal binding properties of monosubstituted ferrocenoyl peptides with thioether-containing sidechains. *Journal of organometallic chemistry* 2011, *696* (3), 715-721.
22. Chandrasoma, A.; Hamid, A. A. A.; Bruce, A. E.; Bruce, M. R. M.; Tripp, C. P., An infrared spectroscopic based method for mercury(II) detection in aqueous solutions. *Analytica Chimica Acta* 2012, *728*, 57-63.
23. Morikawa, G.; Suzuka, C.; Shoji, A.; Shibusawa, Y.; Yanagida, A., High-throughput determination of octanol/water partition coefficients using a shake-flask method and novel two-phase solvent system. *Journal of Pharmaceutical and Biomedical Analysis* 2016, *117*, 338-344.
24. Andersson, J. T.; Schrader, W., A method for measuring 1-octanol - Water partition coefficients. *Analytical Chemistry* 1999, *71* (16), 3610-3614.
25. Hughes, J. D.; Blagg, J.; Price, D. A.; Bailey, S.; DeCrescenzo, G. A.; Devraj, R. V.; Ellsworth, E.; Fobian, Y. M.; Gibbs, M. E.; Gilles, R. W.; Greene, N.; Huang, E.; Krieger-Burke, T.; Loesel, J.; Wager, T.; Whiteley, L.; Zhang, Y., Physiochemical drug properties associated with in vivo toxicological outcomes. *Bioorganic & Medicinal Chemistry Letters* 2008, *18* (17), 4872-4875.
26. Lapic, J.; Havaic, V.; Sakic, D.; Sankovic, K.; Djakovic, S.; Vrcek, V., Ferrocenoyl-Substituted Pyrimidine Nucleobases: An Experimental and Computational Study of Regioselective Acylation of Uracil, Thymine, and 5-Fluorouracil. *European Journal of Organic Chemistry* 2015, (24), 5424-5431.
27. Babij, N. R.; McCusker, E. O.; Whiteker, G. T.; Canturk, B.; Choy, N., NMR Chemical Shifts of Trace Impurities: Industrially Preferred Solvents Used in Process and Green Chemistry. *Organic process research & development 20* (3), 661-667.
28. Yamaguchi, Y.; Ding, W.; Sanderson, C. T.; Borden, M. L.; Morgan, M. J.; Kutal, C., Electronic structure, spectroscopy, and photochemistry of group 8 metallocenes. *Coordination Chemistry Reviews* 2007, *251* (3-4), 515-524.
29. Bozak, R. E., Photochemistry in the Metallocenes. *Advances in Photochemistry* 1971, *8*, 227-244.
30. Ferrus, R.; Egea, M. R., LIMIT OF DISCRIMINATION, LIMIT OF DETECTION AND SENSITIVITY IN ANALYTICAL SYSTEMS. *Analytica Chimica Acta* 1994, *287* (1-2), 119-145.

Author's Biography

Grace Gould was born in Waterville, Maine, on September 2, 1994. She graduated from Waterville Senior High School with high honors in 2012, and began her undergraduate career at the University of Maine as a biology major, switching to chemistry with a concentration in pre-pharmacy studies after a semester. She is a member of Phi Beta Kappa, participates in the American Chemical Society Student Chapter as Vice President, as well as the Screamin' Black Bear Pep Band. She has received a fellowship from the Center for Undergraduate Research for the 2015-2016 academic year.

Upon graduation, Grace will be attending Husson University to pursue a dual Doctor of Pharmacy/Master of Business Administration degree. With her dual degree, she hopes to become employed as medication counselor for individuals in recovery from substance-abuse.